Production of antibodies against ganglioside complexes

In GBS and related disorders subsequent to *C. jejuni* infection, anti-ganglioside antibodies are shown to be induced by the immune reaction against lipo-oligosaccharides (LOS) of pathogens causing antecedent infection (Willison and Yuki 2002; Van Doorn *et al.* 2008). A similar mechanism can be speculated in the production of anti-GSC antibodies. Kuijf *et al.* (2007) recently reported that such anti-GSC antibodies as anti-GM1/GD1a and GQ1b/GD1a cross-reacted to LOS from the autologous *C. jejuni* strain, indirectly demonstrating that the LOS contained GSC-like structures. However, carbohydrate structures expressed in the LOS may not exactly be the combination of the two carbohydrate chains expected from the reactivity of the serum anti-GSC antibodies.

Inhibition of the reactivity of the anti-ganglioside antibody by another coexistent ganglioside

If the interaction of two gangliosides creates a new epitope with conformational changes, the binding acitivity of the antibody highly specific to one ganglioside may be lessened by the addition of another ganglioside to make an antigen mixture.

We investigated sera from 17 GBS patients who had IgG antibody reactive only with GD1b in routine antibody assay. For those sera, antibody activity against a mixture of GD1b and another ganglioside was examined and compared the activity with that against GD1b alone. The results showed that the addition of GD1a, GT1a, GT1b, GQ1b and GalNAc–GD1a to GD1b caused marked decrease of the binding activity of anti-GD1b antibodies, suggesting that those gangliosides may interact with GD1b to make a novel epitope which cannot be easily recognized by the anti-GD1b antibodies (Kaida *et al.* 2008b).

In addition, the reduction rates of the binding activities caused by the addition of such gangliosides as GD1a, GT1b, GQ1b and GalNAc–GD1a were significantly more in the antibodies from ataxic patients than in those from non-ataxic patients. The addition of another ganglioside may cause conformational change. Therefore, the more specific the antibody is, the more affected its reactivity should be. It therefore suggests that the anti-GD1b IgG antibodies in ataxic patients may be more specific to GD1b than those in patients without ataxia. This may provide further evidence to the association between anti-GD1b antibody and ataxia (Kusunoki *et al.* 1996).

Thus, the antibodies specific to GD1a/GD1b complex are associated with severe GBS (Fig. 2) and those specific to GD1b itself are associated with the development of ataxia (Fig. 3).

A similar inhibitory effect of neighboring gangliosides has recently been reported in the case of anti-GM1 antibodies by

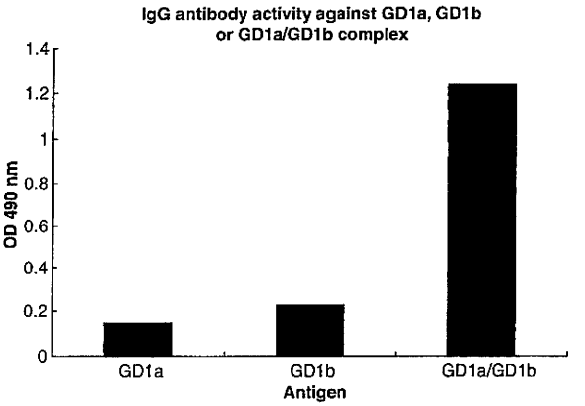

Fig. 2 ELISA result on a serum sample from a patient with severe Guillain-Barré syndrome (Kaida *et al.* 2004). This patient's serum IgG shows strong reaction with a mixture of GD1a and GD1b (GD1a/GD1b) but reacts only weakly with GD1a or GD1b alone.

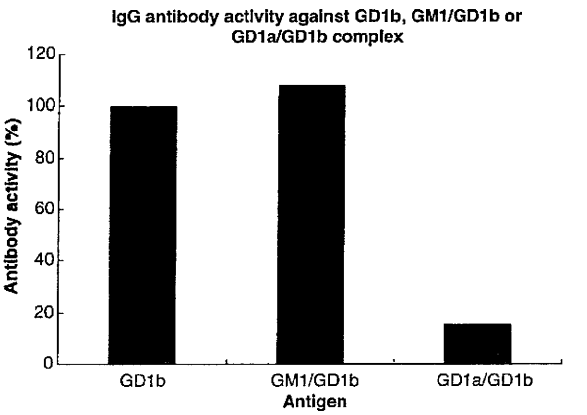

Fig. 3 The IgG antibody activities to mixture antigens in sera from nine GBS patients with ataxia who had only IgG anti-GD1b antibody in routine antibody assay (Kaida *et al.* 2008b). Bars of GM1/GD1b and GD1a/GD1b showed the average activities of the nine patients. Compared with the antibody activity to GD1b alone (100%), the activity was markedly reduced because of the addition of GD1a to GD1b antigen whereas the addition of GM1 did not affect the antibody activity.

Greenshields *et al.* (2009). Negative effects by gangalioside complexes on the binding of IgM anti-GM1 antibodies in sera from patients with chronic immune-mediated neuropathies, particularly multifocal motor neuropathy, have also been reported (Nobile-Orazio *et al.* 2010).

Future studies on the anti-GSC antibodies in the pathogenesis of autoimmune neuropathies

Gangliosides are located in the cell membranes with carbohydrate portions on the outer surfaces, and are preferentially

packaged with cholesterol, forming lipid rafts. Within rafts, gangliosides are considered to interact with important transmembrane receptors or signal transducers (Simons and Ikonen 1997; Hakomori 2002). Anti-GSC antibodies may cause dysfunction of the axon or Schwann cells through their binding to clustered epitopes of glycosphingolipids in the plasma membrane microdomains. Future study on the localization of each ganglioside complex is needed. Animal model of the autoimmune neuropathy mediated by anti-GSC antibodies should also be developed. Such investigations may lead to the understanding of the roles of GSCs in the plasma membrane and of the clinical relevance of the anti-GSCs antibodies.

Acknowledgements

This work was supported by the Ministry of Education, Culture, Sports, Science and Technology of Japan (Grants-in-Aid for Scientific Research, 21390273) and the Ministry of Health Labour, and Welfare of Japan (Health and Labour Sciences Research Grants for Research on intractable diseases (Neuroimmunological Diseases) (H20-016) and for Comprehensive Research on Disability Health and Welfare, H21-012).

References

Capasso M., Caporale C. M., Pomilio F., Gandolfi P., Lugaresi A. and Uncini A. (2003) Acute motor conduction block neuropathy: another Guillain-Barré syndrome variant. *Neurology* **61**, 617–622.

Chiba A., Kusunoki S., Shimizu T. and Kanazawa I. (1992) Serum IgG antibody to gangalioside GQ1b is a possible marker of Miller Fisher syndrome. *Ann. Neurol.* **31**, 677–679.

Chiba A., Kusunoki S., Otaba H., Machinami R. and Kanazawa I. (1993) Serum anti-GQ1b IgG antibody is associated with ophthalmoplegia in Miller Fisher syndrome and Guillain-Barré syndrome: clinical and immunohistochemical studies. *Neurology* **43**, 1911–1917.

Greenshields K. N., Halstead S. K., Zitman F. M. *et al.* (2009) The neuropathic potential of anti-GM1 autoantibodies is required by the local glycolipid environment in mice. *J. Clin. Invest.* **119**, 595–610.

Hadden R. D. M., Cornblath D. R., Hughes R. A., Zielasek J., Hartung H. P., Toyka K. V. and Swan A. V. (1998) Electrophysiological classification of Guillain-Barré syndrome: clinical associations and outcome: Plasma Exchange/Sandoglobulin Guillain-Barré Syndrome Trial Group. *Ann. Neurol.* **44**, 780–788.

Hakomori S. (2002) The glycosynapse. *Proc. Natl Acad. Sci. USA* **99**, 225–232.

Ho T. W., Mishu B., Li C. Y., Gao C. Y., Cornblath D. R., Griffin J. W., Asbury A. K., Blaser M. J. and McKhann G. M. (1995) Guillain-Barré syndrome in northern China. Relationship to *Campylobacter jejuni* infection and anti-glycolipid antibodies. *Brain* **118**, 597–605.

Kaida K., Kusunoki S., Kamakura K., Motoyoshi K. and Kanazawa I. (2000) Guillain-Barré syndrome with antibody to a ganglioside, *N*-acetylgalactosaminyl GD1a. *Brain* **123**, 116–124.

Kaida K., Morita D., Kanzaki M., Kamakura K., Motoyoshi K., Hirakawa M. and Kusunoki S. (2004) Ganglioside complexes as new target antigens in Guillain-Barré syndrome. *Ann. Neurol.* **56**, 567–571.

Kaida K., Kanzaki M., Morita D., Kamakura K., Motoyoshi K., Hirakawa M. and Kusunoki S. (2006) Anti-ganglioside complex antibodies in Miller Fisher syndrome. *J. Neurol. Neurosurg. Psychiatry* **77**, 1043–1046.

Kaida K., Morita D., Kanzaki M., Kamakura K., Motoyoshi K., Hirakawa M. and Kusunoki S. (2007) Anti-ganglioside complex antibodies associated with severe disability in GBS. *J. Neuroimmunol.* **182**, 212–218.

Kaida K., Sonoo M., Ogawa G., Kamakura K., Ueda-Sada M., Arita M., Motoyoshi K. and Kusunoki S. (2008a) GM1/GalNAc–GD1a complex: a target for pure motor Guillain-Barré syndrome. *Neurology* **71**, 1683–1690.

Kaida K., Kamakura K., Ogawa G., Ueda M., Motoyoshi K., Arita M. and Kusunoki S. (2008b) GD1b-specific antibody induces ataxia in Guillain-Barré syndrome. *Neurology* **71**, 196–201.

Kanzaki M., Kaida K., Ueda M., Morita D., Hirakawa M., Motoyoshi K., Kamakura K. and Kusunoki S. (2008) Ganglioside complexes containing GQ1b as targets in Miller Fisher and Guillain-Barre syndrome. *J. Neurol. Neurosurg. Psychiatry* **79**, 1148–1152.

Kuijf M. L., Godschalk P. C., Gilbert M., Endtz H. P., Tio-Gillen A. P., Ang C. W., van Doorn P. A. and Jacobs B. C. (2007) Origin of ganglioside complex antibodies in Guillain-Barré syndrome. *J. Neuroimmunol.* **188**, 69–73.

Kusunoki S., Shimizu J., Chiba A., Ugawa Y., Hitoshi S. and Kanazawa I. (1996) Experimental sensory neuropathy induced by sensitization with ganglioside GD1b. *Ann. Neurol.* **39**, 424–431.

Kusunoki S., Chiba A. and Kanazawa I. (1999) Anti-GQ1b IgG antibody is associated with ataxia as well as ophthalmoplegia. *Muscle Nerve* **22**, 1071–1074.

Kusunoki S., Kaida K. and Ueda M. (2008) Antibodies against gangliosides and ganglioside complexes in Guillain-Barré syndrome: new aspects of research. *Biochim. Biophys. Acta* **1780**, 441–444.

Liu J.-X., Willison H. J. and Pedrosa-Domellof F. (2009) Immunolocalization of GQ1b and related gangliosides in human extraocular neuromuscular junctions and muscle spindles. *Invest. Ophthalmol. Vis. Sci.* **50**, 3226–3232.

Nobile-Orazio E., Giannotta C. and Briani C. (2010) Anti-ganglioside complex IgM antibodies in multifocal motor neuropathy and chronic immune-mediated neuropathies. *J. Neuroimmunol.* **219**, 119–122.

Ogawa G., Kaida K., Kusunoki S., Ueda M., Kimura F. and Kamakura K. (2009) Antibodies to ganglioside complexes consisting of asialo-GM1 and GQ1b or GT1a in Fisher and Guillain-Barre syndromes. *J. Neuroimmunol.* **214**, 125–127.

Simons K. and Ikonen E. (1997) Functional rafts in cell membranes. *Nature* **387**, 569–572.

Van Doorn P., Ruts L. and Jacobs B. (2008) Clinical features, pathogenesis, and treatment of Guillain-Barré syndrome. *Lancet Neurol.* **7**, 939–950.

Willison H. J. and Yuki N. (2002) Peripheral neuropathies and anti-glycolipid antibodies. *Brain* **125**, 2591–2625.

Cellular/Molecular

N-Acetylglucosamine 6-*O*-Sulfotransferase-1-Deficient Mice Show Better Functional Recovery after Spinal Cord Injury

Zenya Ito,[1,2] Kazuma Sakamoto,[1]* Shiro Imagama,[1,2]* Yukihiro Matsuyama,[2] Haoqian Zhang,[1] Kenichi Hirano,[2] Kei Ando,[2] Toshihide Yamashita,[3] Naoki Ishiguro,[2] and Kenji Kadomatsu[1,4]

Departments of [1]Biochemistry and [2]Orthopedics, Nagoya University Graduate School of Medicine, Nagoya 466-8550, Japan, [3]Department of Molecular Neuroscience, Graduate School of Medicine, Osaka University, Osaka 565-0871, Japan, and [4]Institute for Advanced Research, Nagoya University, Nagoya 464-8601, Japan

Neurons in the adult CNS do not spontaneously regenerate after injuries. The glycosaminoglycan keratan sulfate is induced after spinal cord injury, but its biological significance is not well understood. Here we investigated the role of keratan sulfate in functional recovery after spinal cord injury, using mice deficient in *N*-acetylglucosamine 6-*O*-sulfotransferase-1 that lack 5D4-reactive keratan sulfate in the CNS. We made contusion injuries at the 10th thoracic level. Expressions of *N*-acetylglucosamine 6-*O*-sulfotransferase-1 and keratan sulfate were induced after injury in wild-type mice, but not in the deficient mice. The wild-type and deficient mice showed similar degrees of chondroitin sulfate induction and of CD11b-positive inflammatory cell recruitment. However, motor function recovery, as assessed by the footfall test, footprint test, and Basso mouse scale locomotor scoring, was significantly better in the deficient mice. Moreover, the deficient mice showed a restoration of neuromuscular system function below the lesion after electrical stimulation at the occipito-cervical area. In addition, axonal regrowth of both the corticospinal and raphespinal tracts was promoted in the deficient mice. *In vitro* assays using primary cerebellar granule neurons demonstrated that keratan sulfate proteoglycans were required for the proteoglycan-mediated inhibition of neurite outgrowth. These data collectively indicate that keratan sulfate expression is closely associated with functional disturbance after spinal cord injury. *N*-acetylglucosamine 6-*O*-sulfotransferase-1-deficient mice are a good model to investigate the roles of keratan sulfate in the CNS.

Introduction

Neurons in the adult mammalian CNS do not spontaneously regenerate after injuries. Many factors contribute to this lack of repair, including a lack of growth-promoting factors (Widenfalk et al., 2001), the poor intrinsic regenerative capacity of CNS neurons (Neumann and Woolf, 1999), inhibitory factors associated with CNS myelin (Filbin, 2003; McGee and Strittmatter, 2003; Schwab, 2004), chemorepulsive molecules (De Winter et al., 2002), and glial scar-associated inhibitors such as chondroitin sulfate (CS) proteoglycans (CSPGs) (Silver and Miller, 2004).

The extracellular matrix of the adult CNS has a unique composition. Instead of collagens, laminin-1, and fibronectin, this matrix is rich in hyaluronic acid and CSPGs (Ruoslahti, 1996). CSPGs are reinduced after injury and inhibit neuronal axon regrowth. The inhibitory function of CSPGs on axonal outgrowth is primarily ascribed to their covalently attached CS-glycosaminoglycans, since the ablation of CS by use of chondroitinase ABC or a DNA enzyme that acts on xylosyltransferase enhances neuronal axon growth in CNS injury (Moon et al., 2001; Bradbury et al., 2002; Grimpe and Silver, 2004). For example, the axon growth of dopamine neurons is enhanced by chondroitinase ABC treatment after nigrostriatal tract transaction (Moon et al., 2001). Chondroitinase ABC treatment has been shown to enhance functional recovery after spinal cord injury in a rat model (Bradbury et al., 2002). It is known that CSPGs activate the Rho–Rho kinase pathway via an unknown receptor, leading to suppression of axonal growth (Borisoff et al., 2003; Mueller et al., 2005).

Keratan sulfate (KS) is another glycosaminoglycan. It is composed of repeating disaccharide units of galactose and *N*-acetylglucosamine (GlcNAc), where the C6 position of GlcNAc is always sulfated. The 5D4 antibody is commonly used for detection of KS, and it has been demonstrated that 5D4-reactive KS is induced in a rat model of spinal cord injury (Jones and Tuszynski, 2002). The reaction sequence for the biosynthesis of KS consists of *N*-acetylglucosaminylation, 6-sulfation of a GlcNAc residue exposed at the nonreducing end, and galactosylation (Habuchi et al., 2006; Kitayama et al., 2007). Because GlcNAc sulfation at the C6 position is necessary for KS chain elongation (Kitayama et al., 2007), failure of this sulfation leads to loss of KS synthesis. That is, deficiency of human *N*-acetylglucosamine 6-*O*-sulfotransferase-5 (GlcNAc6ST-5) leads to loss of corneal KS synthesis (Akama et al., 2000), and lack of mouse GlcNAc6ST-1 causes loss of 5D4-reactive KS expression in the CNS (Zhang et

Received June 2, 2009; revised Dec. 15, 2009; accepted March 8, 2010.

This work was supported in part by Ministry of Education, Culture, Sports, Science and Technology (MEXT) Grants-in-Aid 18390099 and 20390092 to K.K.; by funds from the 21st Century Centers of Excellence (COE) Program and Global COE Program of MEXT to Nagoya University; and by the Uehara Foundation. We thank T. Muramatsu (Aichi Gakuin University, Nagoya, Japan) for continuous support of this study.

*K.S. and S.I. contributed equally to this work.

Correspondence should be addressed to Kenji Kadomatsu, Department of Biochemistry, Nagoya University Graduate School of Medicine, 65 Tsurumai-cho, Aichi 466-8550, Japan. E-mail: kkadoma@med.nagoya-u.ac.jp.

DOI:10.1523/JNEUROSCI.2570-09.2010

 0270-6474/10/305937-11$15.00/0

al., 2006). In this study, to investigate the biological significance of KS in neurological function, we applied a contusion spinal cord injury model to *N*-acetylglucosamine 6-*O*-sulfotransferase-1-deficient mice and found that these mice showed better functional recovery than their wild-type counterparts.

Materials and Methods

Mice. GlcNAc6ST-1−/− mice were produced using D3 embryonic stem cells and an ordinary gene-targeting technology as described previously (Hemmerich et al., 2001). GlcNAc6ST-1+/− mice obtained after backcrossing with C57BL/6J for more than 11 generations were interbred. The littermates obtained were used for the spinal cord injury experiments. These mice were maintained in the animal facilities of Nagoya University. All experiments were performed in accordance with protocols approved by the institutional animal committee.

Spinal cord injury model. We anesthetized adult C57BL/6J mice, their wild-type littermates, and GlcNAc6ST-1−/− mice (female, 8 weeks old, 20–30 g) using an intraperitoneal injection of pentobarbital sodium (50 mg/kg). After laminectomy at the 10th thoracic spinal lamina, we exposed the dorsal surface of the dura mater. A bilateral contusion injury was created by delivering a 100 kdyn force to the cord using a commercially available spinal cord injury device (Infinite Horizon Impactor; Precision Systems and Instrumentation). Sham controls were subjected to laminectomy only. As postoperative care, the bladder was compressed by manual abdominal pressure twice per day until bladder function was restored, and prophylactic antibiotic treatment [1.0 ml of Bactramin (Roche) in 500 ml of acidified water] was maintained for 1 week. The numbers of mice used and mortality are summarized in supplemental Table 1 (available at www.jneurosci.org as supplemental material).

Reagents. Anti-KS 5D4 and anti-CS CS-56 monoclonal antibodies were purchased from Seikagaku. A biotin labeling kit-NH2 was used for biotinylation of the 5D4 antibody and purchased from Dojindo Molecular Technologies. CD11b monoclonal antibody was from BioLegend; Cy3-conjugated anti-glial fibrillary acidic protein (GFAP) monoclonal antibody was from Sigma; anti-Iba1 polyclonal rabbit antibody was from Wako; anti-platelet-derived growth factor receptor (PDGFr) polyclonal rabbit antibody was from Thermo Fisher Scientific Anatomical Pathology; anti-GAP-43 polyclonal rabbit antibody was from Millipore Bioscience Research Reagents; anti-serotonin (5HT) polyclonal rabbit antibody was from ImmunoStar; anti-type IV collagen polyclonal rabbit antibody was from LSL; and protein kinase Cγ was from Santa Cruz Biotechnology. Cy3- or Cy2-conjugated streptavidin and Cy3-conjugated anti-mouse IgM were from Jackson ImmunoResearch; Cy3-conjugated anti-rabbit IgG was from Zymed; and fluorescein isothiocyanate (FITC)-conjugated anti-rat IgG was from Sigma. FluorSave was obtained from Calbiochem.

Immunohistochemistry. Mice were perfused transcardially under deep ether anesthesia with buffered 4% paraformaldehyde. The spinal cords were removed, postfixed in 4% paraformaldehyde overnight, and cryoprotected in buffered 30% sucrose during the subsequent night. Tissues were cut into 12 μm sections with a cryostat and mounted on glass slides. Sections were blocked in PBS containing 3% bovine serum albumin (BSA) and 5% normal mouse serum for staining of biotin-conjugated anti-KS 5D4 or blocked in PBS containing 1% BSA and 10% normal goat serum for other immunohistochemistry. Sections were then incubated with the primary antibodies at 100× dilution in a blocking solution overnight at 4°C in PBS containing 3% BSA and 5% normal mouse serum or overnight at 4°C in 1% BSA and 10% normal goat serum. After rinsing in PBS, the sections were incubated with the secondary antibody (Cy3- or Cy2-conjugated streptavidin, 1:100; Cy3-conjugated goat anti-rabbit IgG, 1:100; Cy3-conjugated goat anti-mouse IgM, 1:100; or FITC-conjugated goat anti-rat IgG, 1:100) for 60 min at room temperature. Subsequently, the sections were rinsed in PBS, mounted with FluorSave, and examined by confocal microscopy (MRC 1024; Bio-Rad). GAP-43 staining was performed using 3,30-diaminobenzidine (Wako).

Anterograde labeling of the cortico-spinal tract. Eight weeks after injury, descending corticospinal tract (CST) fibers were labeled with biotin-dextran amine (BDA; 10% in saline; 3.2 μl per cortex; molecular weight, 10,000; Invitrogen) injected under anesthesia at the left and the right motor cortices (coordinates: 2 mm posterior to the bregma, 2 mm lateral to the bregma, 0.5 mm depth). For each injection, 0.2 μl of BDA was delivered for a period of 30 s via a 15–20-μm-inner-diameter glass capillary attached to a microliter syringe (ITO). Two weeks after BDA injection, the animals were killed by perfusion with PBS followed by 4% paraformaldehyde. The spinal cords were dissected, postfixed overnight in the same fixatives, and cryopreserved in 30% sucrose in PBS. A 20 mm length of spinal cord 10 mm rostral and 10 mm caudal to the lesion site was embedded in Tissue Tek OCT. These blocks were sectioned in the transverse plane (25 μm). Sections were blocked in PBS with 0.3% Triton X-100 for 4 h and incubated for 2 h with Alexa Fluor 488-conjugated streptavidin (1:400; Invitrogen) in PBS with 0.05% Tween 20. We then took serial cross sections of the spinal cord and performed quantitative analysis of the distribution of the axons. Degrees of BDA uptake were assessed by counting the total number of fibers in the cross section 5 mm rostral to the lesioned site, where the CST was intact. For quantification of the number of labeled corticospinal axons 5 mm caudal to the lesion site, the number of labeled fibers was counted in the gray matter and divided by the number of labeled corticospinal axons 10 mm above the lesion for each animal. The labeled fibers were counted using MetaMorph software. Light intensity and thresholding values were maintained at constant levels for all analyses.

Reverse transcription-PCR. The forward primer 5′-AAGCCTACAGGTGGTGCGAA-3′ and reverse primer 5′-CAGGACTGTTAACCCGCTCA-3′ were used for reverse transcription (RT)-PCR for GlcNAc6ST-1 expression, and the forward primer 5′-GGTGGAGGTCGGAGTCAACG-3′ and reverse primer 5′-CAAAGTTGTCATGGATGACC-3′ were used for RT-PCR for glyceraldehyde 3-phosphate dehydrogenase (GAPDH) expression. SuperScript III reverse transcriptase (Invitrogen) was used to synthesize cDNA.

Morphometry. The epicenter of a lesion was determined by hematoxylin and eosin staining of several of the serial 12 μm sections. All the image analyses were performed using spinal cord samples prepared from six sagittal sections at 12 μm intervals (three sections on either side of the midline, which was identified by the appearance of the central tube), and all the axial image analyses in Figure 6 were performed using spinal cord samples from positions 5 mm caudal to the lesion site. Statistical analyses were performed for five mice for each experimental group. To count reactive astrocytes, standardized areas for sampling in six sections from each animal in each group were identified as a 600-μm-wide band of spinal cord adjoining the cord–lesion interface in each section.

Mean values for each animal were then compared. Light intensity and thresholding values were maintained at constant levels for all analyses by a computer-driven microscope stage (MetaMorph Offline version 6.3 r^2; Molecular Devices). The amounts of fibrous tissue and axonal outgrowth of the wound area were assessed by counting signals visualized by staining with anti-type IV collagen, CD11b, CS-56, GAP-43, and 5HT antibodies, respectively, for 640 × 2200 μm^2 counting frames around a lesion. Data were collected for at least five mice with each genotype in each experiment.

Footfall test. Mice were subjected to the grid runway test to assess locomotor function recovery at 6 weeks after injury. Performance on a wire grid was evaluated for 3 min by counting footfalls. A footfall was defined as either hindpaw missing a rung and extending through the space between adjacent grids. The wire grid was positioned flat and was 7 × 11 inches with grid squares of 0.35 × 0.35 inches. The number of footfalls was counted for five mice in each group.

Footprint test. In the footprint analysis, the hindpaws were covered with ink to record walking patterns during continuous locomotion across a paper runway (1.2 × 12 inches) at 6 weeks after injury, and the stride lengths were calculated. Strides were analyzed only when mice ran with constant velocity. All strides on the first and last 5 cm of the passage were excluded because of changing velocity.

Behavioral testing. The locomotor performance of animals was analyzed using the Basso mouse scale (BMS) open-field score (Basso et al., 2006) for 8 weeks, since the BMS has been shown to be a valid locomotor rating scale for mice. The evaluations were made by two blind observers for all analyzed groups. Briefly, the BMS is a nine-point scale that pro-

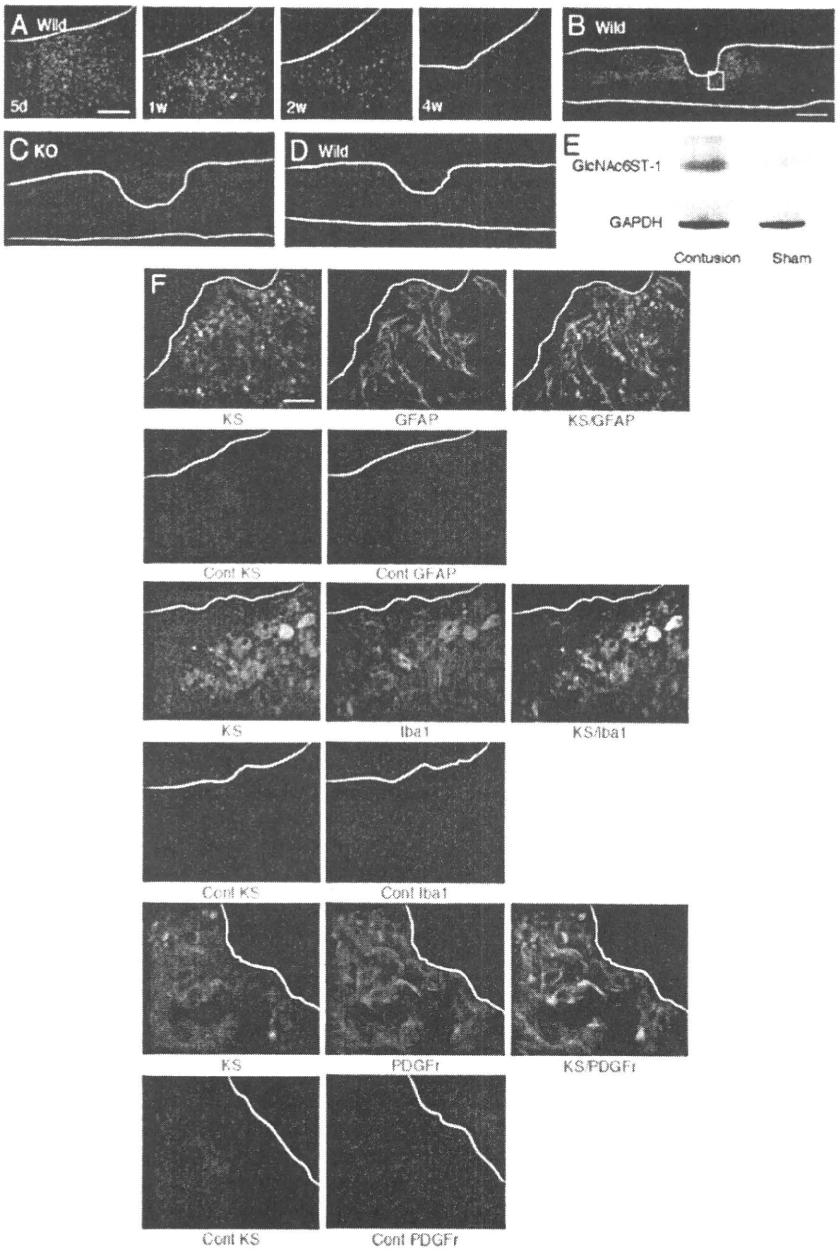

Figure 1. KS expression after spinal cord injury. ***A***, Expression profile of 5D4-reactive KS in wild-type mice after spinal cord injury. Scale bar, 100 μm. d, Day; w, week. ***B–D***, KS was expressed around the lesion center 7 d after injury in wild-type mice (***B***) but was not detected in GlcNAc6ST-1−/− mice (KO; ***C***) or isotype-matched IgG controls (***D***). ***E***, RT-PCR for GlcNAc6ST-1 and GAPDH was performed for samples from the wild-type mouse spinal cord 7 d after injury or sham operation. ***F***, Double staining for KS and a glial cell marker. Reactive astrocytes (GFAP), microglia (Iba1), and oligodendrocyte precursors (PDGF receptors) were examined. Scale bar, 50 μm. The sections shown are midline sagittal sections of the injured spinal cord. The drawn lines indicate the margins of the lesion core (***A***) and the outline of the spinal cord (***B***, ***C***).

vides a gross indication of locomotor ability and determines the phases of locomotor recovery and features of locomotion. The BMS score was determined for seven mice in each group.

Electrophysiology. In terminal electrophysiological experiments, after an intraperitoneal injection of ketamine (100 mg/kg), short trains of five square-wave stimuli of 0.5 ms duration with an interstimulus interval of 2 ms were delivered through the occipito-cervical area by small electrode balls, and needle electrodes were placed in both hindlimbs. The active electrode was placed in the muscle belly, and the reference electrode was placed near the distal tendon of the muscle in each limb. The ground electrode was placed subcutaneously between the coil and the recording electrodes. The onset latency was measured as the length of time in milliseconds between the stimulus and the onset of the first wave. One hundred responses were averaged and stored for off-line analysis of latency.

Cell culture. Sprague Dawley rats at postnatal days 7–9 were killed, and the cerebella were collected. The meninges were carefully removed with fine forceps, and the remaining tissues were minced and digested using a Papain Dissociation System (Worthington). Dissociated cells were applied to a 35/60% two-step Percoll gradient and centrifuged at 3000 × *g* for 15 min. Cerebellar granule neurons at the interface were collected. Cells were suspended in Neurobasal medium (Invitrogen) supplemented with 2% B27 (Invitrogen), 2 mM glutamine, an additional 20 mM KCl, 50 U/ml penicillin, and 50 μg/ml streptomycin.

Substrate preparation. Four-well chamber slides (NUNC) were coated with 20 μg/ml poly-L-lysine (PLL; Sigma) and left overnight at 4°C and then were coated with chick brain proteoglycans (Millipore Bioscience Research Reagents) or the other indicated substrates and left for 4 h at 37°C. If indicated, proteoglycans were treated with 200 mU/ml chondroitinase ABC or 5 mU/ml keratanase II derived from *Bacillus* sp. Ks36 (Seikagaku) in PBS at 37°C. Other substrate materials included poly-L-ornithine, myelin-associated glycoprotein (Sigma), Nogo, oligodendrocyte myelin glycoprotein (R & D Systems), KS and chondroitin sulfate C (Seikagaku).

Cell adhesion assay. Cerebellar granule neurons were seeded onto chick proteoglycan-coated chamber slides at 2.0×10^5 per well. After 2 h, nonadherent cells were washed out with PBS, and adherent cells were visualized by nuclear staining with 4′,6-diamidino-2-phenylindole (DAPI). The number of adherent cells was counted under 200× magnification (six fields).

Neurite outgrowth assays. Cerebellar granule neurons were seeded onto four-well chamber slides at 2.0×10^5 per well. Twenty-four hours after seeding, the neurons were fixed with 4% paraformaldehyde/PBS and stained with anti-neuron-specific β-tubulin (Covance) to visualize neurites. Neurite lengths were measured from at least 100 neurons that had neurites longer than twice the cell body diameter, per condition from duplicate wells, and quantified as described previously (Ughrin et al., 2003).

Isolation and purification of proteoglycans from mouse brains. Whole brains were isolated from C57BL/6J mice (postnatal day 5). Tissues were homogenized in PBS containing 10 mM *N*-ethylmaleimide and protease inhibitor mixtures (Nacalai Tesque) using a Dounce-type homogenizer. Homogenates were centrifuged at 24,000 × *g* for 30 min, and supernatants were applied to DEAE-Sepharose (GE Healthcare). Samples were washed three times with wash buffer (50 mM Tris-HCl, pH 7.5, 2 M urea, 0.25 M NaCl, 20 mM EDTA, 0.2 mM PMSF, 1 mM *N*-ethylmaleimide), and the proteoglycans were eluted with 2 M NaCl. The eluent was concentrated using a size-exclusion spin column (molecular weight cutoff, 100 kDa), and the protein concentration was determined using a Micro BCA Protein Assay kit (Thermo Fisher Scientific).

Spot assay. PLL-coated chamber slides were air dried and spotted with 5 μl of proteoglycans (10 μg/ml) from mouse brains. The spotted area was visualized by staining with rhodamine B (10 μg/ml). If indicated, proteoglycans were predigested with keratanase (500 mU/ml) and keratanase II (5 mU/ml) at 37°C for 2 h before spotting. Cerebellar granule neurons were seeded onto four-well chamber slides at 1.0×10^5 or 1.0×10^6 per well.

Coating efficiency. Five microliters of aggrecan (50 μg/ml), which had been treated with or without keratanase (500 mU/ml) and keratanase II (5 mU/ml) at 37°C for 2 h, were spotted onto PLL-coated chamber slides. After overnight incubation at 37°C, the coated aggrecan was visualized using an anti-CS antibody (CS56), followed by Alexa-488-conjugated anti-mouse IgM antibody.

Statistical analysis. Statistical analyses were performed with an unpaired two-tailed Student's *t* test for single comparisons and one-way ANOVA for multiple comparisons. For the footfall and footprint scores, repeated-measures ANOVA and the Mann–Whitney *U* test were used. In all statistical analyses, values of $p < 0.05$ were considered to indicate significance. To obtain the data for statistical analyses, the investigators were blinded to the genotypes in all procedures.

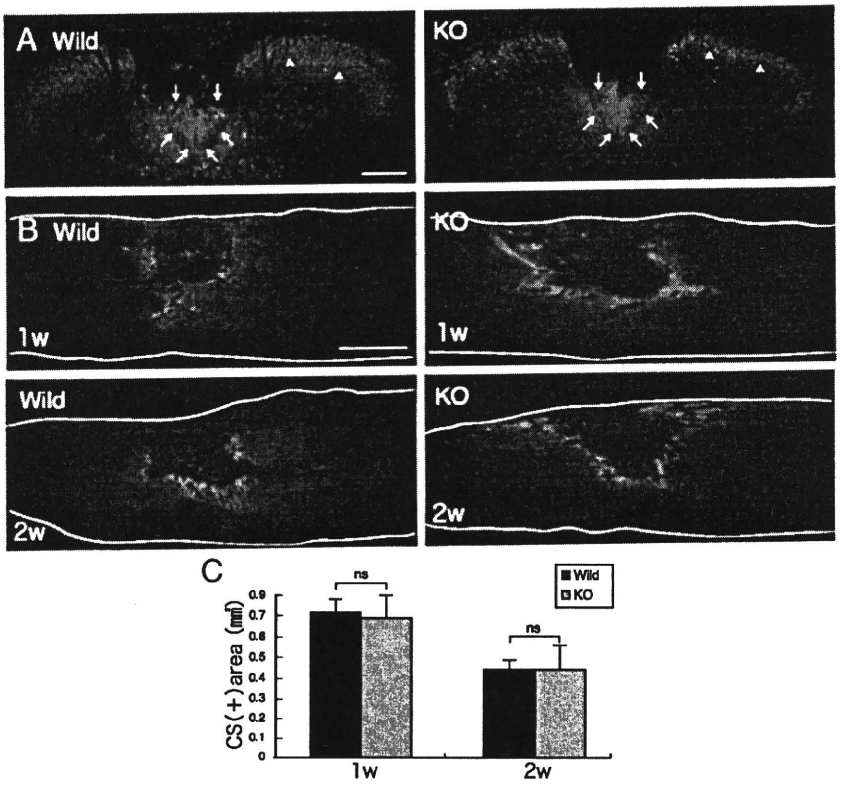

Figure 2. CST and CS expression after injury. *A*, The CST was stained with anti-protein kinase C-γ antibody (arrow). Densely packed immunofluorescent small cells are located in the inner part of lamina II of the substantia geratinosa (arrowhead) on the axial section. Scale bar, 200 μm. The sections shown are axial sections of the injured spinal cord. *B*, CS expression was determined with CS-56 antibody. Scale bar, 500 μm. The sections shown are the midline sagittal sections of the injured spinal cord. The drawn lines indicate the outline of the spinal cord. *C*, Quantification of CS expression. Five mice for each genotype at each time point were examined. Quantification data are the means ± SEM. ns, Not significant (Student's *t* test). w, Week; KO, knock-out.

Results

Induction of KS expression after spinal cord injury in wild-type mice

We used a contusion injury model of the spinal cord to investigate the significance of KS in neurological function after injuries. The contusion injury of the spinal cord was made at the 10th thoracic level with 100 kdyn using an Infinite Horizon Impactor. To reveal the expression and localization of KS, 5D4, an anti-KS monoclonal antibody, was used. 5D4-reactive KS expression was induced around the core lesion, reached a maximum level around 5–7 d after injury in wild-type mice (Fig. 1*A*), and was not detected at all in GlcNAc6ST-1−/− mice (Fig. 1*B–D*). GlcNAc6ST-1 expression was also enhanced in injured wild-type mice (Fig. 1*E*).

Antibodies against GFAP, Iba1, and PDGFr were used to identify KS-expressing cells. 5D4-reactive KS did not overlap GFAP, but a portion of the Iba1-positive cells overlapped 5D4-reactive cells (Fig. 1*F*). Almost all PDGFr-positive cells were 5D4 positive (Fig. 1*F*). These data indicated that KS was mainly expressed by oligodendrocyte precursor cells (PDGFr positive) and partially expressed by microglia (Iba1 positive), which is consistent with the 5D4-reactive KS expression previously reported in a rat spinal cord injury model (Jones and Tuszynski, 2002).

CST, CS expression, and inflammatory cell accumulation

Protein kinase C-γ is a marker for the CST. Protein kinase C-γ immunoreactivity was observed in the dorsal column and lamina II of the spinal cords of uninjured mice (Fig. 2*A*, arrows and arrowheads, respectively) at the T5 level of the cord. The immunoreactivity was similar in wild-type and GlcNAc6ST-1−/− mice (Fig. 2*A*), and the BMS locomotor score before spinal cord injury was also similar in both groups (data not shown), indicating that the CST had formed in a normal fashion in GlcNAc6ST-1−/− mice and thus that these mice could be used for the motor function analyses.

In contrast to KS expression, CS expression in GlcNAc6ST-1−/− mice as judged by CS-56 immunoreactivity was comparable to that in wild-type mice (Fig. 2*B*,*C*). Furthermore, CD11b (a marker of monocytes/macrophages and granulocytes)-positive inflammatory cells were accumulated in the lesion to a similar extent in wild-type and GlcNAc6ST-1−/− mice (data not shown).

Motor function

We next evaluated functional recovery after injury. The footfall test and footprint test were used to objectively evaluate motor function. For the footfall test, mice were placed on a lattice of thin metal wires. This test requires accurate limb placement and precise motor control. Intact animals cross the grid without making footfalls, whereas a paralytic foot tends to fall from the lattice during movement. The numbers of footfalls were comparable between wild-type and GlcNAc6ST-1−/− mice 3 d after injury (Fig. 3*A*). GlcNAc6ST-1−/− mice gradually recovered and, at 4–6 weeks after injury, showed footfall counts comparable to those of sham-operated mice (Fig. 3*A*). In contrast, wild-type mice still showed frequent footfalls at 4 and 6 weeks after injury (Fig. 3*A*; see movie in supplemental Fig. S1, available at www.jneurosci.org as supplemental material).

On the footprint test, GlcNAc6ST-1−/− mice showed a well balanced and organized walk at 4 weeks after injury, whereas wild-type mice showed a disorganized walk, sometimes with toe drop (Fig. 3*B*, arrow). The profiles of stride length deduced

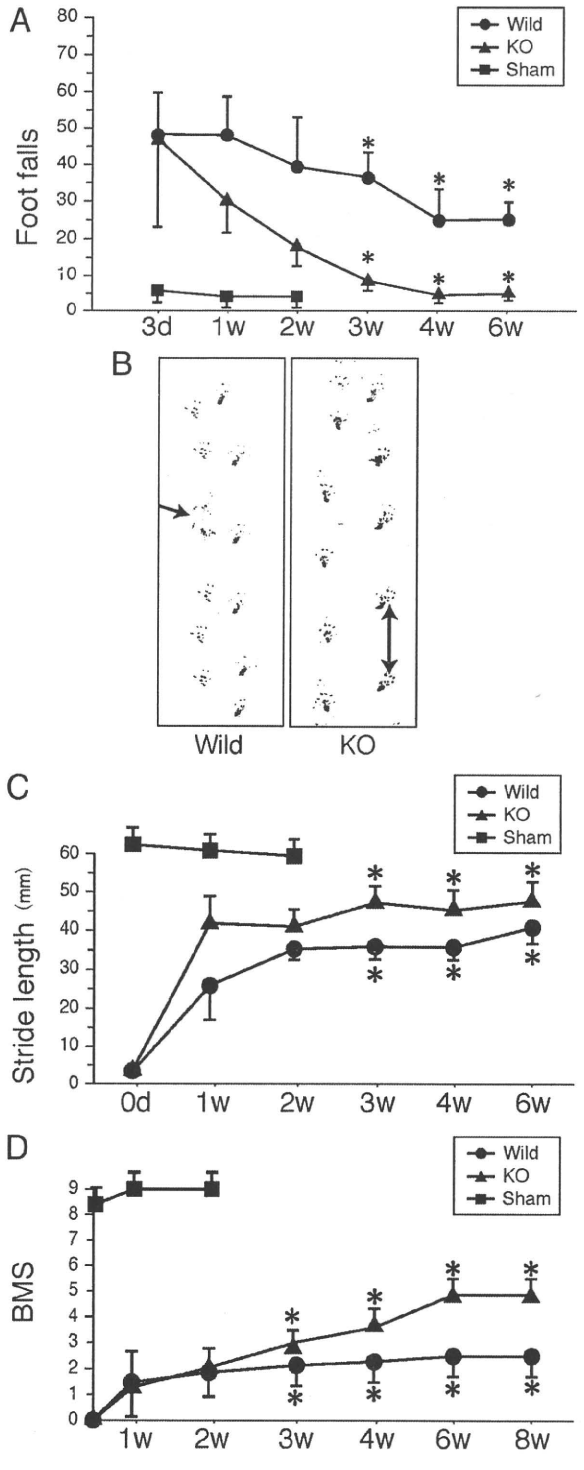

Figure 3. Footfall and footprint tests and BMS scoring. ***A***, Footfall test. The graph shows data from five mice for each genotype at each time point. ***B***, Representative photos of the footprint test taken 4 weeks after injury. The arrow indicates a toe drop. ***C***, Data of the footprint test are quantified. Five mice were used for each genotype at each time point. Quantification data are the means ± SEM (repeated-measures ANOVA and the Mann–Whitney *U* test). ***D***, BMS scoring. The graph shows data from seven mice for each genotype at each time point. $*p < 0.05$ (wild-type vs GlcNAc6ST-1−/− mice). d, Day; w, week; KO, knock-out.

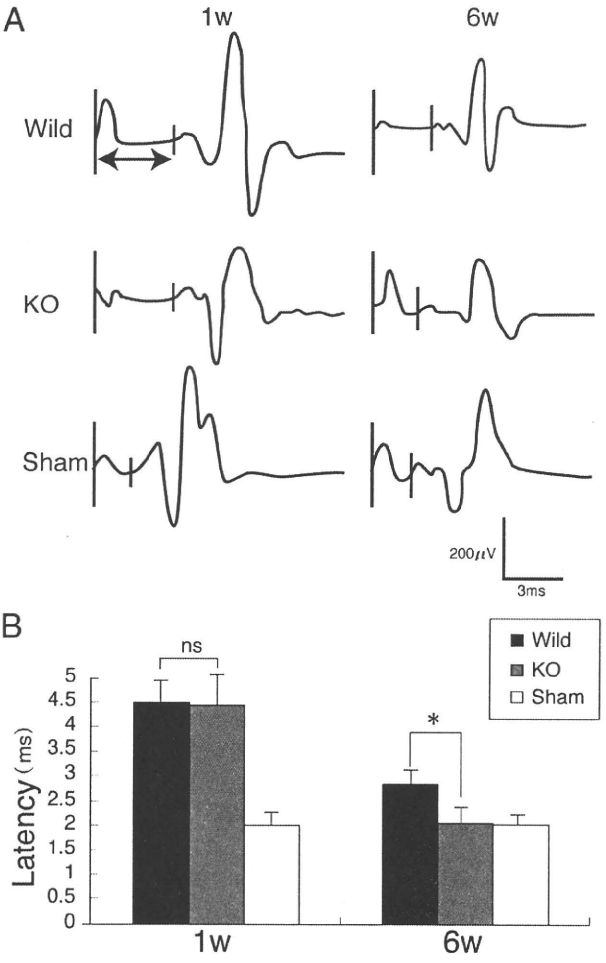

Figure 4. Motor-evoked potential. ***A***, Representative profiles of motor-evoked potentials are shown. ***B***, Latency times were quantified. Five mice were used for each genotype at each time point. $*p < 0.05$. Quantification data are the means ± SEM (one-way ANOVA). W, week; KO, knock-out; ns, not significant.

from the footprints clearly demonstrated that the recovery of motor function was significantly better in GlcNAc6ST-1−/− mice (Fig. 3*C*).

We also performed BMS locomotor scoring for 8 weeks. There was a significantly better recovery in the GlcNAc6ST-1−/− mice than in the wild-type controls (Fig. 3*D*). These data were consistent with those of our footfall scoring and footprints, in which a significant recovery was observed from 3 weeks after the spinal cord injury (Fig. 3*B–D*). Using the same mice as used for BMS scoring, we also examined the footfall test results over a longer period (supplemental Fig. S2 and Table 1, available at www.jneurosci.org as supplemental material) and confirmed the reproducibility of the data in Figure 3*A*. These mice were also compared with hemisection and total section models as described below.

Next, to confirm that our 100 kdyn contusion model inflicted an injury of sufficient severity, we subjected additional mice to total section and hemisection injuries and compared their motor function with that of our 100 kdyn contusion injury model. In the footfall test, the hemisection model showed a substantial degree of spontaneous recovery, reaching an almost normal level 6 weeks after spinal cord injury, whereas the total section model showed a severe motor function disturbance even 6 weeks after injury. The 100 kdyn contusion injury was more severe than the

hemisection injury but milder than the total section injury (supplemental Fig. S2, available at www.jneurosci.org as supplemental material). Furthermore, in the BMS scores of wild-type mice, we did not observe spontaneous recovery of motor function even 8 weeks after contusion injury (Fig. 3*D*). Together, these results suggest that our contusion model was sufficiently severe and was appropriate for evaluating functional recovery after spinal cord injury.

Motor-evoked potential has been widely used in clinical and animal trials of spinal cord injury to evaluate the neuromuscular system function. In the present work, the latency of motor-evoked potential was measured to also objectively evaluate motor function. Mice received electrical stimuli at the occipito-cervical area, and the motor-evoked potential was recorded at both hindlimbs. The latency of the motor-evoked potential was measured from the onset of the stimulus to the first response of each wave. At 1 week after injury, the latency was elongated to a similar extent in wild-type and GlcNAc6ST-1−/− mice, but at 6 weeks after injury, the latency of GlcNAc6ST-1−/− mice became comparable to that of the sham-operated controls, whereas that of wild-type mice was significantly longer (Fig. 4). These data support the conclusion that functional recovery was significantly better in GlcNAc6ST-1−/− mice.

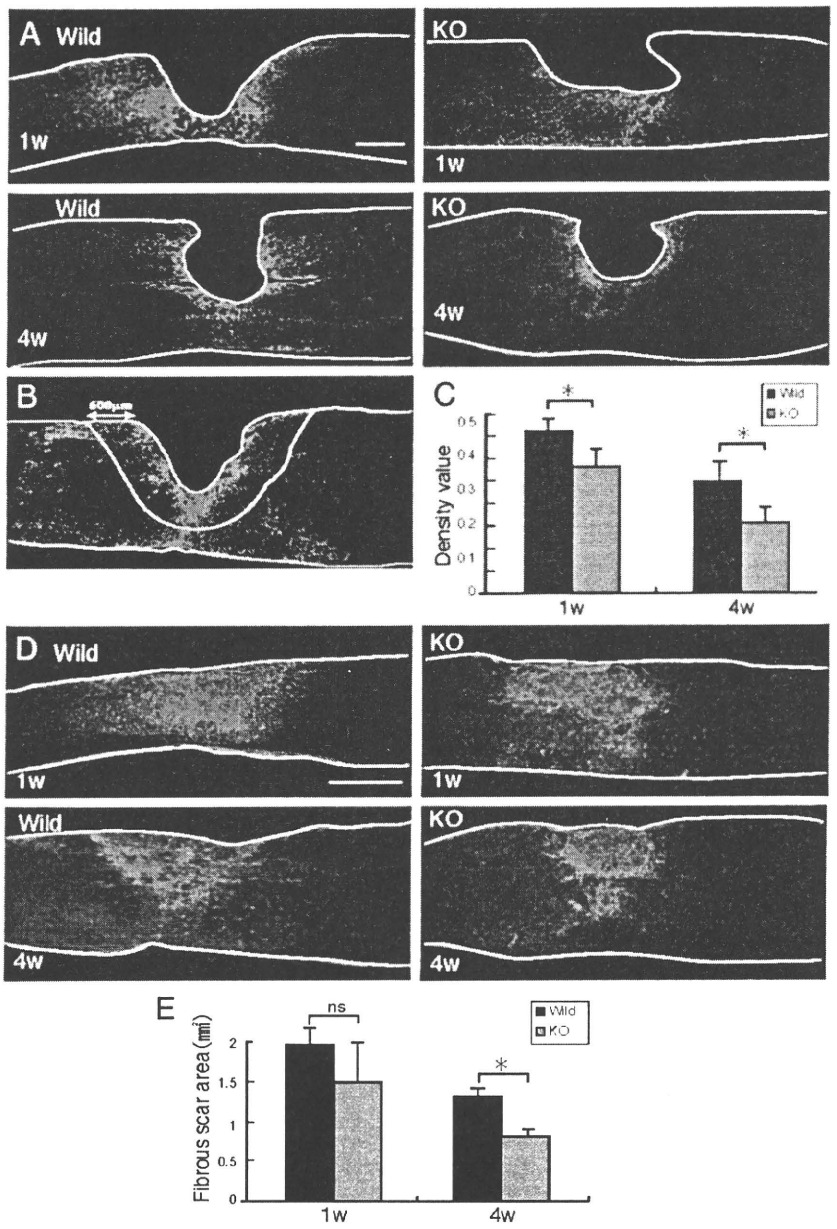

Figure 5. Reactive astrocyte accumulation and collagen IV deposition. ***A***, Representative photos for GFAP expression are shown. Scale bar, 500 μm. The drawn lines indicate the margins of the lesion core and the outline of the spinal cord. ***B***, The GFAP-positive area in a field of 600 μm width around the lesion center (lack of GFAP signal) was measured. The drawn lines indicate the outline of the spinal cord and the measured area. ***C***, The GFAP-positive area is summarized in the graph. Five mice were used for each genotype at each time point. $*p < 0.05$. ***D***, Representative photos for collagen IV expression are shown. Scale bar, 500 μm. The drawn lines indicate the outline of the spinal cord. ***E***, The collagen IV-positive areas are summarized in the graph. Five mice were used for each genotype at each time point. $*p < 0.05$. Quantification data are the means ± SEM (Student's *t* test). The sections shown are midline sagittal sections of the injured spinal cord. W, week; KO, knock-out; ns, not significant.

Glial scar formation

We next examined glial scar formation. Accumulation of GFAP-positive reactive astrocytes appeared after injury in both wild-type and GlcNAc6ST-1−/− mice. However, their accumulation was weaker in GlcNAc6ST-1−/− mice than in wild-type mice: the GFAP-positive area in a region of 600 μm width around the lesion core was significantly smaller in GlcNAc6ST-1−/− mice (Fig. 5*A–C*). An important marker for glial scarring is collagen IV, which appears in the late stages of glial scarring (Liesi and Kauppila, 2002). In the present study, collagen IV expression in the injured area became apparent 7 d after injury in both wild-type and GlcNAc6ST-1−/− mice, but the margin was unclear. There was no difference in scar area (the collagen IV-positive area) between the two genotypes. The margin of the scar area became clear at 4 weeks after injury, and the scar area was significantly reduced in GlcNAc6ST-1−/− mice (Fig. 5*D,E*).

Neuronal axon growth

Regeneration of the serotonergic descending raphespinal tract may partly explain the reason for motor function recovery after spinal cord injury in rodents (Kim et al., 2004). We stained tissues 5 mm distal to the lesion for 5-hydroxytryptamine (5HT), since serotonergic axons are 5HT positive. 5HT-positive fibers were more abundantly found in the ventral horn of the gray matter in GlcNAc6ST-1−/− mice than in wild-type mice (5HT-positive area: wild-type, 972 ± 1080 vs GlcNAc6ST-1−/−, 7120 ± 1168 μm^2; $p < 0.005$) (Fig. 6*A–C*). Positive GAP-43 staining reflects axon regeneration and sprouting (Tetzlaff and Bisby, 1989; King et al., 2001). GAP-43-positive axons were also much more abun-

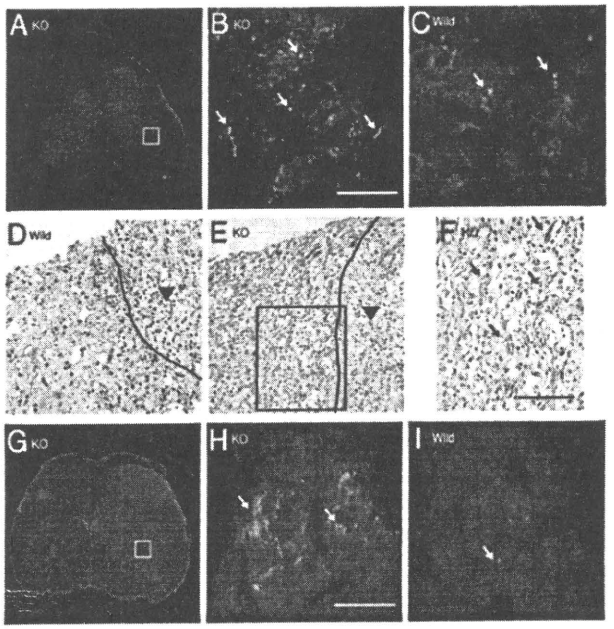

Figure 6. Axonal growth. 5HT staining of the ventral horn (***A–C***; 5 mm distal to the lesion), GAP43 staining (***D–F***), and tracer-fiber counts of the CST (BDA-positive fibers) (***G–I***; 5 mm caudal to the lesion) are shown for GlcNAc6ST-1−/− (***A***, ***B***, ***E–H***) and wild-type (***C***, ***D***, ***I***) mice. Scale bar, 50 μm. Higher-magnification figures of the boxed areas in ***A***, ***E***, and ***G*** are shown in ***B***, ***F***, and ***H***, respectively. The arrows in ***B***, ***C***, ***F***, ***H***, and ***I*** indicate 5HT-, GAP43-, and BDA-positive fibers, respectively. The arrowheads in ***D*** and ***E*** indicate the contusion area. The drawn lines indicate the margins of the lesion core. Five mice were used for each genotype at 4 weeks after injury. The sections in ***A–C***, ***G***, ***H***, and ***I*** are the axial sections of the injured spinal cord. The sections in ***D–F*** are the midline sagittal sections of the injured spinal cord. KO, Knock-out.

dant in GlcNAc6ST-1−/− mice than in wild-type mice at 4 weeks after injury (GAP-43-positive fiber counts/150,000 μm^2: wild-type, 1962 ± 1522 vs GlcNAc6ST-1−/−, 6631 ± 1090; $p < 0.005$) (Fig. 6*D–F*). Moreover, we investigated axonal growth in the CST. In tracer-fiber counts for the CST, the number of BDA-positive fibers was increased in the region caudal to the epicenter in GlcNAc6ST-1−/− mice, particularly in the gray matter in this region (Fig. 6*G–I*). For quantification of the number of labeled BDA, the number of labeled fibers was counted in the gray matter 5 mm caudal to the lesion and divided by the number of labeled corticospinal axons 10 mm rostral to the lesion for each animal. There was a significant difference between wild-type and GlcNAc6ST-1−/− mice (BDA-positive fibers in caudal region/rostral region: wild-type, 1.9 ± 1.1% vs GlcNAc6ST-1−/−, 6.9 ± 1.0%; $p < 0.005$).

Chondroitinase ABC promotes collateral sprouting of spared fibers in the cuneate nucleus after cervical spinal cord injury (Massey et al., 2006), suggesting that proteoglycans limit not only axon regeneration but also sprouting. Our data on 5HT staining, GAP-43 staining, and CST tracer-fiber counts are in line with this idea.

Requirement of KS for the proteoglycan-mediated inhibition of neurite growth

To further explore the underlying mechanisms involving KS in the functional disturbance, we performed *in vitro* experiments. We first asked whether KS was sufficient to inhibit neurite growth. However, glycosaminoglycans (KS and CS), whether administered singly or in combination, did not inhibit neurite outgrowth (Fig. 7*A*). Thus, we focused on the role of KS chains on proteoglycans.

Proteoglycans purified from the brains of chicks contained both KS and CS, because the 5D4-reactive smear appeared more strongly after the CS-degrading enzyme chondroitinase ABC treatment, and the smear disappeared after keratanase II treatment on Western blot analysis (Fig. 7*B*). As it is known that proteoglycans inhibit not only neurite outgrowth but also cell adhesion to the substrate (Kaneko et al., 2007), we examined whether the proteoglycans used in this study would inhibit cell–substrate adhesion. As shown in Figure 7, *C* and *D*, the number of cells adhered to the substrate decreased as the concentration of coated proteoglycans increased. However, if the proteoglycan concentration was lower than 300 ng/ml, the number of cells adhering to the proteoglycans was comparable to the number adhering to the PLL-coated slides (Fig. 7*C*,*D*). Therefore, we decided to use the condition of 300 ng/ml proteoglycans for coating in the neurite outgrowth assay, so that we could discriminate the effect of proteoglycans on neurite outgrowth from that on cell–substrate adhesion.

Proteoglycans coated on the substratum strikingly inhibited the neurite outgrowth of primary neurons compared with the PLL control (Fig. 7*E*,*F*). Molecules derived from myelin, such as Nogo, myelin-associated glycoprotein, and oligodendrocyte-myelin glycoprotein, are known as strong *in vivo* inhibitors of axonal regrowth. Our *in vitro* assay showed that these molecules also inhibit the neurite outgrowth of primary granular neurons from the rat cerebellum (Fig. 7*F*). Notably, the KS-degrading enzyme keratanase II blocked the proteoglycan-mediated inhibition, and this blocking effect was comparable to that of chondroitinase ABC (Fig. 7*E*,*F*).

Finally, we developed an assay system, the spot assay, and used it to examine the activity of mouse brain proteoglycans. We first confirmed that the mouse brain proteoglycans indeed contained both KS and CS (Fig. 8*A*). We then spotted these proteoglycans with rhodamine B, so that the spots appeared red (Fig. 8*B*). Whereas neurites of the primary neurons frequently crossed into the spots in the control (rhodamine B alone) (Fig. 8*B*, top), neurites of neurons in the surrounding area did not enter into the spots of the mouse brain proteoglycans (Fig. 8*B*, middle). However, if the proteoglycans were treated with keratanase, neurites of neurons in the surrounding area could enter the spots (Fig. 8*B*, bottom). This phenomenon was more clearly demonstrated if the seeded cell number was decreased (Fig. 8*C*). Therefore, this *in vitro* assay using brain proteoglycans mimicked the *in vivo* failure of axonal regrowth into the lesions of spinal cord injury and the reversal of this failure in KS-deficient mice.

To examine the possibility that keratanase decreases the efficiency of proteoglycan binding to the substrate, we used the KS/CSPG aggrecan for spotting and visualized spots with the anti-CS antibody CS56. However, we did not observe any difference between spots with and without predigestion with keratanase (supplemental Fig. S3, available at www.jneurosci.org as supplemental material).

Discussion

There have been only a few studies on the relationship between KS and the nervous system. KS expression is induced in the injured CNS after cortical stab wounds in neonatal rats and in the postcomissural fornix after lesioning in adult rats (Geisert and Bidanset, 1993; Stichel et al., 1999). KS expression is also enhanced in reactive microglia and oligodendrocyte progenitors after rat spinal cord injury (Jones and Tuszynski, 2002). After

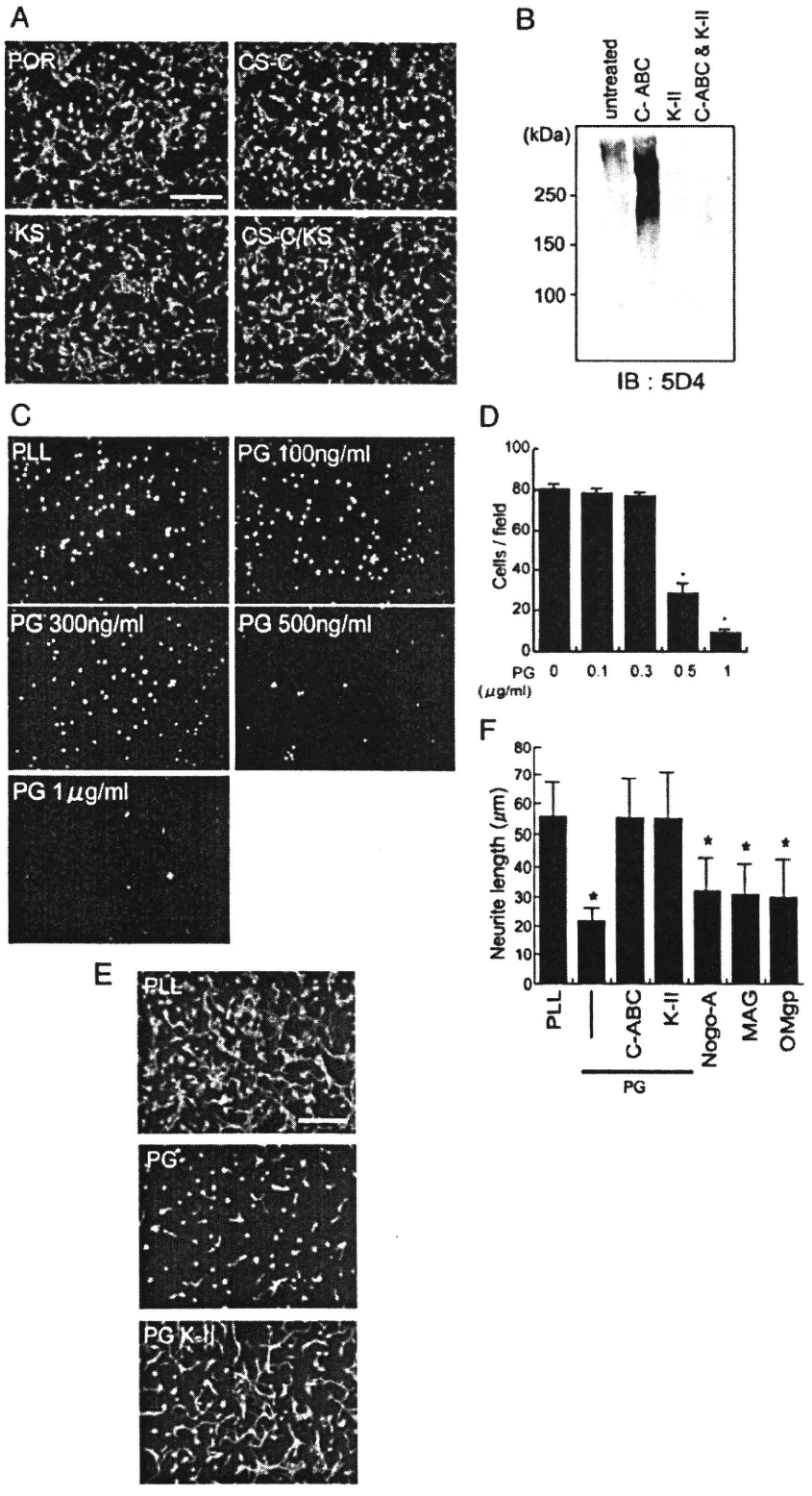

Figure 7. Requirement of KS for the proteoglycan-mediated inhibition of neurite outgrowth. ***A***, Postnatal day 8 (P8) rat cerebellar granule neurons were cultured on poly-L-ornithine (POR), POR plus chondroitin sulfate C (CS-C) (20 μg/ml), or POR plus KS (20 μg/ml). Scale bar, 100 μm. ***B***, Chick brain proteoglycans contained KS. Chick brain proteoglycans (CC117; Millipore) were digested with chondroitinase ABC (C-ABC; 500 mU/ml), keratanase II (K-II; 5 mU/ml), or both and subjected to Western blot analysis. Note that C-ABC treatment revealed KS epitopes. ***C***, P8 rat cerebellar granular neurons were cultured on PLL or proteoglycan (PG) extracted from chick brains. To count adhered cells, the nucleus was stained with DAPI, and the cell number was counted for six fields under 200× magnification. ***D***, The quantification of ***C***. Data represent the average cell number ± SD. *$p <$ 0.01, versus 0 μg of PG. ***E***, P8 rat cerebellar granular neurons were cultured on PLL or PG extracted from chick brains. Keratanase II treatment restored the neurite outgrowth. Scale bar, 100 μm. ***F***, The quantification of ***E***. Data represent the average neurite length ± SD. *$p < 0.05$ versus PLL. PG (300 ng/ml), C-ABC (200 mU/ml), K-II (5 mU/ml), Nogo (800 ng/ml), myelin-associated glycoprotein (MAG) (400 ng/ml), and oligodendrocyte myelin glycoprotein (OMgp) (400 ng/ml) were used.

unilateral axotomy of the nigrostriatal tract in adult rats, CSPGs and keratan sulfate proteoglycans (KSPGs) are predominantly found in the lesion surround where reactive astrocytes, activated microglia, and adult precursor cells are abundant (Moon et al., 2002). We previously found enhanced axonal growth in cortical stab wounds in GlcNAc6ST-1−/− mice, but we were not able to investigate the neurological function of these mice at that time (Zhang et al., 2006). In the present study, GlcNAc6ST-1−/− mice exhibited better motor function recovery and enhanced regeneration of the serotonergic descending raphespinal tract axons and CST axons after spinal cord injury, compared with wild-type mice. In support of these data, we also found that the KS-degrading enzyme keratanase reversed the proteoglycan-mediated inhibition of neurite outgrowth *in vitro*. In light of these results, the present study is the first to demonstrate a possible link between KS and neurological function and indicates that GlcNAc6ST-1−/− mice are a good model for investigating the roles of KS in the CNS.

It is of note that neither CS nor KS was sufficient to inhibit neurite outgrowth *in vitro*. However, CS or KS degradation blocked the inhibitory activity of proteoglycans both from chick brains and mouse brains. These results suggest that KS is required for the proteoglycan-mediated inhibition of neurite outgrowth. To our surprise, the effect of KS degradation on this inhibition was comparable to that of CS degradation. Thus, it will be interesting to ask whether KS degradation also promotes functional recovery after neuronal injuries as CS degradation does.

Among the numerous methods available to assess the recovery of locomotor functions, the Basso, Beattie, and Bresnahan (BBB) locomotor scale is a popular choice, because it measures functional changes in voluntary hindlimb movements. In this study, we first used the BBB locomotor scale using five mice in each group, and although we found a slight difference in recovery between the GlcNAc6ST-1−/− mice and controls, the difference did not reach the level of statistical significance ($p = 0.07$; data not

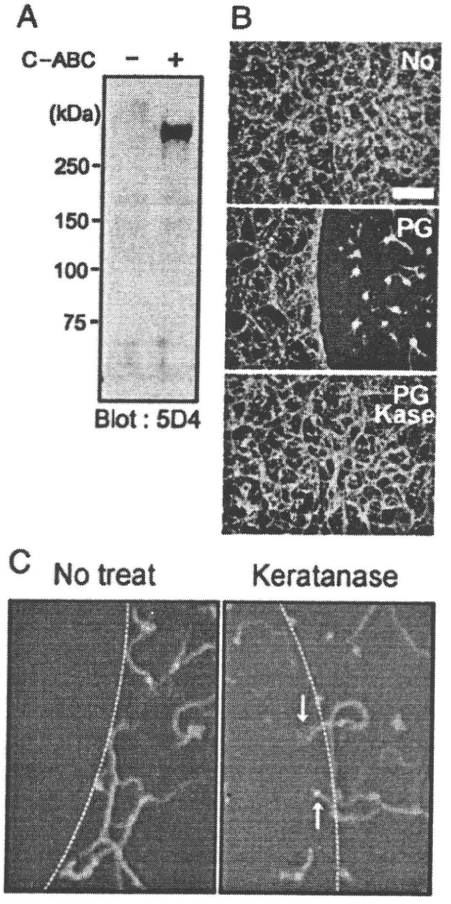

Figure 8. Spot assay. ***A***, Proteoglycans from mouse brain were subjected to Western blot analysis. Note that C-ABC treatment revealed KS epitopes. ***B***, ***C***, Spot assay. Mouse brain proteoglycans at 3 μg/ml were spotted, and primary granular neurons from the rat cerebellum were seeded. Proteoglycans inhibited neurite entry into the spot, whereas keratanase treatment allowed entry. Different cell numbers were used for ***B*** and ***C*** (1.0×10^6 or 1.0×10^5 per well, respectively). Scale bar, 100 μm.

shown). Several locomotor parameters recover differently in mice than in other species (e.g., coordination and paw position recover simultaneously, trunk stability improves earlier, and trunk and hindlimb spasms occur later). These differences limit the sensitivity of the BBB for mice and necessitate a ranking of locomotor attributes unique to mice. To overcome this limitation, a BMS scale was developed for mice (Basso et al., 2006); we applied this locomotor scale using seven mice in each group for 8 weeks and detected a significantly better recovery in the GlcNAc6ST-1−/− mice than in the wild-type controls (Fig. 3*D*). This result was consistent with the footfall, footprint, and motor-evoked potential results. Collectively, the above findings led us to conclude that functional recovery was promoted in GlcNAc6ST-1−/− mice.

The findings of the motor-evoked potential test were consistent with those of the footfall test, footprint test, and BMS scoring. Because the motor-evoked potential test uses only the combination of electric stimulus and response, it can be objectively evaluated. It has recently been shown that motor-evoked potentials have good sensitivity for recording reductions in central conduction latencies (Pluchino et al., 2003; Biffi et al., 2004). In the present study, the responses showed normal configurations, but latency was delayed in the wild-type mice. These electrophysiological data support the idea that the functional recovery of GlcNAc6ST-1−/− mice is remarkably enhanced. However, there may be numerous mechanisms underlying these differences in latency: the conduction differences could be mediated not only by differences in axon regrowth or myelination but also by synaptic reorganization, such as synaptic sprouting, activation of silent synapses, and biochemical synaptic strengthening. Moreover, the type of stimulation used could have activated many descending axon tracts, including not only the CST but also other tracts, such as the rubrospinal, vesitbulospinal, reticulospinal, and propriospinal tracts.

In the present study, we found that most PDGFr-positive cells and a portion of the Iba1-positive cells were KS positive at 7 d after spinal cord injury (Fig. 1). We also found that a portion of the Iba1-positive cells were also KS positive at 3 d, a time point at which most of the Iba1-positive cells were expected to be resident microglia, not macrophages (data not shown). Consistent with this, we have recently reported that primary cultured microglia express KS, and this expression is enhanced by TGF-β, a microglia-activating cytokine usually induced after neuronal injuries (Yin et al., 2009). Considering these results together, it is most likely that, in addition to oligodendrocyte precursor cells (PDGFr positive), activated microglia are a main source of KSPG.

Regarding the reduction of glial scarring in GlcNAc6ST-1−/− mice, whether or not this phenomenon assisted in the functional recovery of these mice is a subject for future debate. Although it is known that glial scars formed in part by reactive astrocytes inhibit axonal sprouting and functional restoration after spinal cord injury (Menet et al., 2003), reactive astrocytes support repair of the blood–brain barrier, prevent inflammatory cell infiltration, and protect neurons and oligodendrocytes (Bush et al., 1999; Faulkner et al., 2004). At least in the subacute phase (within 2 weeks after spinal cord injury), the accumulation of reactive astrocytes helps to repair tissue and restore function (Okada et al., 2006). In this context, our findings are complex. That is, we found that the reactive astrocyte accumulation was significantly lower in GlcNAc6ST-1−/− mice than wild-type mice both at 1 and 4 weeks after injury, whereas the collagen deposition of the GlcNAc6ST-1−/− mice was lower only 4 weeks after injury. It is known that the reactive astrocytes and cells invading into the lesion (i.e., fibroblasts, meningeal cells, and Schwann cells) produce extracellular matrix, including collagen IV (Schwab and Bartholdi, 1996; Fawcett and Asher, 1999; Condic and Lemons, 2002; Buss et al., 2007). However, the influence of collagen IV expression on plasticity and regeneration at the lesion site *in vivo* has been controversial and remains to be elucidated (Shiga and Oppenheim, 1991; Stichel et al., 1999; Weidner et al., 1999; Buss et al., 2007). Thus, our present study has, at least, demonstrated a close association between diminished KS expression and suppressed reactive astrocyte accumulation and collagen IV deposition, although the underlying mechanisms are still elusive.

KS seems to be the most important factor in accounting for the phenotype of GlcNAc6ST-1−/− mice in this study, but we need to exclude the possibility that sulfation modifications on other sugar structures are mediated by GlcNAc6ST-1 and play a role in neuronal function. Other than KS, the only product of GlcNAc6ST-1 thus far identified is sialyl 6-sulfo Le^X, which is a determinant of L-selectin and plays a critical role in lymphocyte recruitment (Uchimura K et al., 2004). GlcNAc sulfation of sialyl 6-sulfo Le^X is mediated either by GlcNAc6ST-1 or -2 (Hemmerich et al., 2001; Uchimura et al., 2004). GlcNAc6ST-1−/− mice show reduced lymphocyte homing to lymph

nodes, and mice doubly deficient in GlcNAc6ST-1 and -2 show significantly greater reduction of lymphocyte homing (Uchimura et al., 2004, 2005; Kawashima et al., 2005). However, we observed a similar degree of CD11b-positive inflammatory cell infiltration in wild-type and GlcNAc6ST-1−/− mice. Therefore, it is not likely that sialyl 6-sulfo Le^X was responsible for the difference in motor function between the wild-type and GlcNAc6ST-1−/− mice in the present study. Furthermore, we obtained evidence that the KS-degrading enzyme keratanase promotes neurite outgrowth, which is inhibited by proteoglycans. Together, our data strongly suggest that the GlcNAc6ST-1 product KS plays a critical role in functional disturbance after spinal cord injury.

References

Akama TO, Nishida K, Nakayama J, Watanabe H, Ozaki K, Nakamura T, Dota A, Kawasaki S, Inoue Y, Maeda N, Yamamoto S, Fujiwara T, Thonar EJ, Shimomura Y, Kinoshita S, Tanigami A, Fukuda MN (2000) Macular corneal dystrophy type I and type II are caused by distinct mutations in a new sulphotransferase gene. Nat Genet 26:237–241.

Basso DM, Fisher LC, Anderson AJ, Jakeman LB, Mctigue DM, Popovich PG (2006) Basso mouse scale for locomotion detects differences in recovery after spinal cord injury in five common mouse strains. J Neurotrauma 23:635–659.

Biffi A, De Palma M, Quattrini A, Del Carro U, Amadio S, Visigalli I, Sessa M, Fasano S, Brambilla R, Marchesini S, Bordignon C, Naldini L (2004) Correction of metachromatic leukodystrophy in the mouse model by transplantation of genetically modified hematopoietic stem cells. J Clin Invest 113:1108–1110.

Borisoff JF, Chan CC, Hiebert GW, Oschipok L, Robertson GS, Zamboni R, Steeves JD, Tetzlaff W (2003) Suppression of Rho-kinase activity promotes axonal growth on inhibitory CNS substrates. Mol Cell Neurosci 2:405–416.

Bradbury EJ, Moon LD, Popat RJ, King VR, Bennett GS, Patel PN, Fawcett JW, McMahon SB (2002) Chondroitinase ABC promotes functional recovery after spinal cord injury. Nature 416:636–640.

Bush TG, Puvanachandra N, Horner CH, Polito A, Ostenfeld T, Svendsen CN, Mucke L, Johnson MH, Sofroniew MV (1999) Leukocyte infiltration, neuronal degeneration, and neurite outgrowth after ablation of scar-forming, reactive astrocytes in adult transgenic mice. Neuron 23:297–308.

Buss A, Pech K, Kakulas BA, Martin D, Schoenen J, Noth J, Brook GA (2007) Growth-modulating molecules are associated with invading Schwann cells and not astrocytes in human traumatic spinal cord injury Brain 130:940–953.

Condic ML, Lemons ML (2002) Extracellular matrix in spinal cord regeneration: getting beyond attraction and inhibition. Neuroreport 13:37–48.

De Winter F, Holtmaat AJ, Verhaagen J (2002) Neuropilin and class 3 semaphorins in nervous system regeneration. Adv Exp Med Biol 515:115–139.

Faulkner RJ, Julia E. Herrmann, Michael J. Woo, Keith E. Tansey, Ngan B. Doan, Michael V. Sofroniew (2004) Reactive Astrocytes Protect Tissue and Preserve Function after Spinal Cord Injury. J Neurosci 24:2143–2155.

Fawcett JW, Asher RA (1999) The glial scar and central nervous system repair. Brain Res Bull 49:377–391.

Filbin MT (2003) Myelin-associated inhibitors of axonal regeneration in the adult mammalian CNS. Nat Rev Neurosci 4:703–713.

Geisert EE Jr, Bidanset DJ (1993) A central nervous system keratan sulfate proteoglycan: localization to boundaries in the neonatal rat brain. Brain Res Dev Brain Res 75:163–173.

Grimpe B, Silver J (2004) Novel DNA enzyme reduces glycosaminoglycan chains in the glial scar and allows microtransplanted dorsal root ganglia axons to regenerate beyond lesions in the spinal cord. J Neurosci 24:1393–1397.

Habuchi H, Habuchi O, Uchimura K, Kimata K, Muramatsu T (2006) Determination of substrate specificity of sulfotransferases and glycosyltransferases (proteoglycans). Methods Enzymol 416:225–243.

Hemmerich S, Bistrup A, Singer MS, van Zante A, Lee JK, Tsay D, Peters M, Carminati JL, Brennan TJ, Carver-Moore K, Leviten M, Fuentes ME, Ruddle NH, Rosen SD (2001) Sulfation of L-selectin ligands by an HEV-restricted sulfotransferase regulates lymphocyte homing to lymph nodes. Immunity 15:237–247.

Jones LL, Tuszynski MH (2002) Spinal cord injury elicits expression of keratan sulfate proteoglycans by macrophages, reactive microglia, and oligodendrocyte progenitors. J Neurosci 22:4611–4624.

Kaneko M, Kubo T, Hata K, Yamaguchi A, Yamashita T (2007) Repulsion of cerebellar granule neurons by chondroitin sulfate proteoglycans is mediated by MAPK pathway. Neurosci Lett 423:62–67.

Kawashima H, Petryniak B, Hiraoka N, Mitoma J, Huckaby V, Nakayama J, Uchimura K, Kadomatsu K, Muramatsu T, Lowe JB, Fukuda M (2005) N-acetylglucosamine-6-O-sulfotransferases 1 and 2 cooperatively control lymphocyte homing through L-selectin ligand biosynthesis in high endothelial venules. Nat Immunol 6:1096–1104.

Kim JE, Liu BP, Park JH, Strittmatter SM (2004) Nogo-66 receptor prevents raphespinal and rubrospinal axon regeneration and limits functional recovery from spinal cord injury. Neuron 44:439–451.

King CE, Canty AJ, Vickers JC (2001) Alterations in neurofilaments associated with reactive brain changes and axonal sprouting following acute physical injury to the rat neocortex. Neuropathol Appl Neurobiol 27: 115–126.

Kitayama K, Hayashida Y, Nishida K, Akama TO (2007) Enzymes responsible for synthesis of corneal keratan sulfate glycosaminoglycans. J Biol Chem 282:30085–30096.

Liesi P, Kauppila T (2002) Induction of type IV collagen and other basement-membrane-associated proteins after spinal cord injury of the adult rat may participate in formation of the glial scar. Exp Neurol 173:31–45.

Massey JM, Hubscher CH, Wagoner MR, Decker JA, Amps J, Silver J, Onifer SM (2006) Chondroitinase ABC digestion of the perineuronal net promotes functional collateral sprouting in the cuneate nucleus after cervical spinal cord injury. J Neurosci 26:4406–4414.

McGee AW, Strittmatter SM (2003) The Nogo-66 receptor: focusing myelin inhibition of axon regeneration. Trends Neurosci 26:193–198.

Menet V, M. Prieto, A. Privat, M. Giménez y Ribotta (2003) Axonal plasticity and functional recovery after spinal cord injury in mice deficient in both glial fibrillary acidic protein and vimentin genes. Proc Natl Acad Sci U S A 100:8999–9004.

Moon LD, Asher RA, Rhodes KE, Fawcett JW (2001) Regeneration of CNS axons back to their target following treatment of adult rat brain with chondroitinase ABC. Nat Neurosci 4:465–466.

Moon LD, Asher RA, Rhodes KE, Fawcett JW (2002) Relationship between sprouting axons, proteoglycans and glial cells following unilateral nigrostriatal axotomy in the adult rat. Neuroscience 109:101–117.

Mueller BK, Mack H, Teusch N (2005) Rho kinase, a promising drug target for neurological disorders. Nat Rev Drug Discov 4:387–398.

Neumann S, Woolf CJ (1999) Regeneration of dorsal column fibers into and beyond the lesion site following adult spinal cord injury. Neuron 23:83–91.

Okada S, Nakamura M, Katoh H, Miyao T, Shimazaki T, Ishii K, Yamane J, Yoshimura A, Iwamoto Y, Toyama Y, Okano H (2006) Conditional ablation of Stat3 or Socs3 discloses a dual role for reactive astrocytes after spinal cord injury. Nat Med 12:829–834.

Pluchino S, Quattrini A, Brambilla E, Gritti A, Salani G, Dina G, Galli R, Del Carro U, Amadio S, Bergami A, Furlan R, Comi G, Vescovi AL, Martino G (2003) Injection of adult neurospheres induces recovery in a chronic model of multiple sclerosis. Nature 422:688–694.

Ruoslahti E (1996) Brain extracellular matrix. Glycobiology 6:489–492.

Schwab ME (2004) Nogo and axon regeneration. Curr Opin Neurobiol 14:118–124.

Schwab ME, Bartholdi D (1996) Degeneration and regeneration of axons in the lesioned spinal cord. Physiol Rev 76:319–370.

Shiga T, Oppenheim RW (1991) Immunolocalization studies of putative guidance molecules used by axons and growth cones of intersegemental interneurons in the chick embryo spinal cord. J Comp Neurol 310:234–252.

Silver J, Miller JH (2004) Regeneration beyond the glial scar. Nat Rev Neurosci 5:146–156.

Stichel CC, Hermanns S, Luhmann HJ, Lausberg F, Niermann H, D'Urso D, Servos G, Hartwig HG, Müller HW (1999) Inhibition of collagen IV deposition promotes regeneration of injured CNS axons. Eur J Neurosci 11:632–646.

Tetzlaff W, Bisby MA (1989) Neurofilament elongation into regenerating facial nerve axons. Neuroscience 29:659–666.

Uchimura K, Kadomatsu K, El-Fasakhany FM, Singer MS, Izawa M, Kannagi R, Takeda N, Rosen SD, Muramatsu T (2004) N-acetylglucosamine 6-O-sulfotransferase-1 regulates expression of L-selectin ligands and lymphocyte homing. J Biol Chem 279:35001–35008.

Uchimura K, Gauguet JM, Singer MS, Tsay D, Kannagi R, Muramatsu T, von Andrian UH, Rosen SD (2005) A major class of L-selectin ligands is eliminated in mice deficient in two sulfotransferases expressed in high endothelial venules. Nat Immunol 6:1105–1113.

Ughrin YM, Chen ZJ, Levine JM (2003) Multiple regions of the NG2 proteoglycan inhibit neurite growth and induce growth cone collapse. J Neurosci 23:175–186.

Weidner N, Grill RJ, Tuszynski MH (1999) Elimination of basal lamina and the collagen "scar" after spinal cord injury fails to augment corticospinal tract regeneration. Exp Neurol 160:40–50.

Widenfalk J, Lundströmer K, Jubran M, Brene S, Olson L (2001) Neurotrophic factors and receptors in the immature and adult spinal cord after mechanical injury or kainic acid. J Neurosci 21:3457–3475.

Yin J, Sakamoto K, Zhang H, Ito Z, Imagama S, Kishida S, Natori T, Sawada M, Matsuyama Y, Kadomatsu K (2009) Transforming growth factor-beta1 upregulates keratan sulfate and chondroitin sulfate biosynthesis in microglia after brain injury. Brain Res 1263:10–22.

Zhang H, Muramatsu T, Murase A, Yuasa S, Uchimura K, Kadomatsu K (2006) N-Acetylglucosamine 6-O-sulfotransferase-1 is required for brain keratan sulfate biosynthesis and glial scar formation after brain injury. Glycobiology 16:702–710.

Neuroscience Letters 488 (2011) 299–304

Contents lists available at ScienceDirect

Neuroscience Letters

journal homepage: www.elsevier.com/locate/neulet

Hyaluronan oligosaccharides promote functional recovery after spinal cord injury in rats

Norimitsu Wakao[a,b], Shiro Imagama[a,b], Haoquian Zhang[c], Ryoji Tauchi[a,b], Akio Muramoto[a,b], Takamitsu Natori[a], Sawako Takeshita[d], Naoki Ishiguro[b], Yukihiro Matsuyama[e], Kenji Kadomatsu[a,*]

[a] Department of Biochemistry, Nagoya University Graduate School of Medicine, 65 Tsurumai-cho, Showa-ku, Nagoya 466-8550, Japan
[b] Department of Orthopedics, Nagoya University Graduate School of Medicine, 65 Tsurumai-cho, Showa-ku, Nagoya 466-8550, Japan
[c] Department of Neurosurgery, University of California, San Francisco, CA 94143-0110, USA
[d] Central Research Laboratories, Seikagaku Corporation, 3-1253 Tateno, Higashiyamato, Tokyo 207-0021, Japan
[e] Department of Orthopedics, Hamamatsu Medical University, 1-20-1 Handayama, Higashi-ku, Hamamatsu 431-3192, Japan

ARTICLE INFO

Article history:
Received 18 September 2010
Received in revised form
17 November 2010
Accepted 17 November 2010

Keywords:
Hyaluronan oligosaccharide
Spinal cord injury
Neuroprotection
Axonal regeneration

ABSTRACT

Hyaluronan is a component of the extracellular matrix of the central nervous system, and forms perineuronal nets around neurons. It has been recently reported that the hyaluronan-degrading enzyme hyaluronidase promotes lateral mobility of AMPA-type glutamate receptors and enhances synaptic plasticity. However, the biological significance of hyaluronan-degrading products (oligosaccharides) has not been studied in depth. Here we investigated the effects of hyaluronan oligosaccharides on motor function recovery after spinal cord injury in rats. The disaccharide HA2 and especially the tetrasaccharide HA4, significantly improved motor function, unlike the case with oligosaccharides composed of 6–12 saccharides. Consistent with this finding, HA4 treatment enhanced axonal regeneration/sprouting, as assessed by corticospinal tract tracer fiber counts. HA4 treatment also significantly suppressed accumulation of Iba-1-positive cells in a lesion two weeks after injury. *In vitro* experiments demonstrated that NMDA-induced neuronal cell death was partly blocked by HA4, but not by other oligosaccharides, whereas proteoglycan-mediated inhibition of neurite outgrowth was not affected by treatment with any oligosaccharide examined. Taken together, the present results revealed that due in part to its neuroprotective activity, HA4 promotes motor function recovery after spinal cord injury.

The extracellular matrix (ECM) surrounding neurons in the central nervous system (CNS) forms a lace-like structure, the so-called perineuronal net (PNN) [20]. PNN is composed of hyaluronan (hyaluronic acid; HA), proteoglycans and tenacin R [17]. The globular domains located in the N-terminal of unique proteoglycans (referred to as "lecticans") bind to HA, and the C-terminal domains of proteoglycans are linked to tenacin R, so that a complex, lace-like structure is formed. Although PNN surrounding GABAergic interneurons is prominent, it can be detected on virtually all neurons [2,3,9]. A recent report suggested that the HA-degrading enzyme hyaluronidase and the chondroitin sulfate-degrading enzyme chondroitinase-ABC enhance the lateral mobility of the AMPA receptor, and consequently promote short-term synaptic plasticity [4]. Considering that chondroitin sulfate proteoglycans are the major type of proteoglycan in the PNN, both hyaluronidase and chondroitinase ABC may degrade various PNN components, and consequently destroy the PNN structure. PNN may thus inhibit structural rearrangements at synapses, and consequently contribute to the maintenance of neuronal networks. This idea is further supported by recent studies showing that chondroitinase-ABC restores the plasticity of not only sensory networks but also of networks associated with emotion [5,14]. However, the hyaluronidase used is a testicular enzyme, and chondroitinase ABC is a bacterial enzyme. Thus, these enzymes are absent in mammalian CNS. Therefore, the proof and characterization of neuronal enzymes, which degrade glycosaminoglycans, are still missing.

In contrast to extensive investigations of the effects of PNN-degrading enzymes on the structural rearrangement of neuronal networks, little attention has been paid to degradation products. In the present study, we investigated biological effects of HA oligosaccharides, preparing HA oligosaccharides composed of 2–12 saccharides (HA2–HA12), and applied them to spinal cord injury

Abbreviations: AMPA, DL-α-amino-3-hydroxy-5-methylisoxazole-4-propionic acid; HA, hyaluronan acid; NMDA, N-methyl-D-aspartic acid; Iba-1, ionized calcium binding adaptor protein; SCI, spinal cord injury; BBB scores, Basso, Beattie and Bresnahan scores; CMF-PBS, calcium–magnesium free PBS; PG, proteoglycans; BSA, bovine serum albumin; CST, corticospinal tract; BDA, biotin-dextran amine.

* Corresponding author. Tel.: +81 52 744 2059; fax: +81 52 744 2065.
E-mail address: kkadoma@med.nagoya-u.ac.jp (K. Kadomatsu).

0304-3940/$ – see front matter © 2010 Elsevier Ireland Ltd. All rights reserved.
doi:10.1016/j.neulet.2010.11.051

sites in a rat model. We observed a prominent functional recovery in animals treated with HA4, and detected HA4 neuroprotective activity.

HA oligosaccharides were prepared according to the method reported previously [21] with minimal modification. Briefly, HA (supplied from Sikagaku Corporation. Tokyo) was depolymerized by partial digestion with testicular hyaluronidase and separated into size-uniform HA oligosaccharides by anion exchange chromatography after removal of hyaluronidase. After desalting by size-exclusion chromatography, the purity and size of each HA oligosaccharide were confirmed by high-performance liquid chromatography (HPLC). Endotoxins, proteins, and DNA were absent in these oligosaccharide preparations. High-molecular-weight hyaluronan (HMW-HA; 600–1200 kd) was purchased from the Seikagaku Biobusiness Corporation (Tokyo, Japan).

Adult female Sprague-Dawley rats weighing 200–230 g were used. The animals were anesthetized with an intraperitoneal injection of ketamine (100 mg/kg) and xylazine (10 mg/kg). After Th9 laminectomy, we exposed the dura mater and induced an injury force, 200 kdyn, with a commercially available spinal cord injury device (Infinite Horizon impactor; Precision Systems & Instrumentation). Immediately after including the spinal cord contusion, we performed a Th12 partial laminectomy, and inserted a thin silicone tube with an osmotic mini-pump into the subarachnoid cavity under a surgical microscope. Osmotic mini-pumps (200 μl solution, 0.5 μl/h, 14-d delivery; Alzet pump model 2002 [Durect Co.]) were filled with each of the oligosaccharides and either HMW-HA (10 μg/200 μl), or saline (as a vehicle control). The tube was sutured to the spinous process to anchor it in place, and the mini-pump was placed under the skin on the animal's back. Afterward, muscles and skin were closed in layers. The bladder was compressed by manual abdominal pressure twice a day until bladder function was restored. All animals were given antibiotics in drinking water (1.0 ml Bactramin [Roche] in 500 ml acidified water) for 2 weeks after SCI. We used animals which showed complete paralysis (BBB score = 0), the day after the operation. Other animals which could move their hind paw or died immediately were excluded.

Recovery of hind-limb motor function was assessed by measuring the Basso, Beattie and Bresnahan (BBB) scores [1]. Quantification was performed in a blinded manner by two observers.

CGNs were prepared from Sprague-Dawley rats on postnatal days 7–8 by essentially using a described method [7,16]. Briefly, the cerebella were cleared of meninges and blood vessels, roughly homogenized by chopping, and trypsinized. Neurons were washed in the presence of DNAse 1 and soybean trypsin inhibitor (Sigma–Aldrich), and cellular debris was pelleted by centrifugation. The starting cell suspension was applied immediately to a two-step gradient of Percoll (35/60% in calcium and magnesium-free PBS containing 2 mM EDTA [Pharmacia Fine Chemicals]). Gradients were centrifuged at 2000 × *g* for 10 min in a clinical centrifuge. The two resulting bands, one at the interface of the CMF-PBS/35% Percoll, and the other at the interface between the layer of 35% Percoll and that of 60% Percoll, were removed with a fire-polished Pasteur pipette, diluted to 10 ml with CMF-PBS, pelleted at 600 rpm for 5 min, washed twice in Neurobasal medium supplemented with B27 (Gibco), and counted.

CGN cultures were plated on 24-well plates (TPP) coated with 0.01% poly-L-lysine (Sigma–Aldrich) at a density of 1.0×10^6 cells/ml. Cells were maintained at 37 °C with 5% CO_2 for 24 h. After cells were kept for 24 h in culture in Neurobasal medium supplemented with B27, cytosine D-arabinoside (Sigma–Aldrich) was added at a final concentration of 10 μg/ml in order to arrest any additional growth of non-neuronal cells. Cultures were supplemented twice per week. At 14 days *in vitro*, we added each of the HA oligo preparations to the neuronal cell cultures 24 h prior to administration of the glutamate analogue, NMDA (Tocris). Concentrations of the HA preparations and NMDA were 10 μg/ml and from 10 to 500 μM. In some experiments, HA oligosaccharides were washed off twice with fresh medium from those cultures pretreated with HA (10 μg/ml) for 24 h, after which NMDA was added to the cultures. After an additional 24 h culture, cells were incubated (37 °C with 5% CO_2, 15 min) with 10 mM propidium iodide (PI; Dojindo), 1 mM calcein-AM (Dojindo), and DAPI (Vector Laboratories), which stained the nuclei of dead cells, viable cells, and all cells, respectively. Then, cells were mounted on coverslipped glass slides. Fluorescent images of each well were inspected and photographed using an inverted phase-contrast microscope (Olympus, Model BX60). The ratio of dead-to-viable cells was calculated using the following formula: (PI positive cells/PI positive cells + calcein-AM positive cells) × 100. In addition, neuronal cell death was estimated by measuring the activity of lactate dehydrogenase (LDH) released from damaged or destroyed cells into the culture media. All LDH activity was measured using an LDH-cytotoxic test kit according to the protocol recommended by the manufacturer (Wako).

All substrates were prepared prior to the assay and stored at −80 °C until needed. CGN cultures were plated on two-chamber poly-L-lysine-(0.01%) coated Lab-Tek slides (Nunc) coated with PG (300 ng/ml) obtained from chicken brain (CC117, Chemicon) with each of the HA oligo at a density of 5.0×10^5 cells/ml. After cells were maintained at 37 °C with 5% CO_2 for 24 h, CGN cultures were fixed in 4% (w/v) paraformaldehyde, followed by blocking in 1% (w/v) BSA and permeabilization with 0.3% Triton X-100 in PBS for 15 min at room temperature. Then, cultures incubated with anti-beta-tubulin class III mouse monoclonal antibody at 1:500 (Tuj-1; Convance) for 1 h. After rinsing, plates were incubated with secondary FITC goat anti-mouse antibodies at 1:100 (Invitrogen). The neurite length per cell was evaluated using an inverted phase-contrast microscope (Olympus, Model BX60). Processes with a length equivalent to one or more diameters of the cell body were considered to reflect neuritis and were measured by Image J software. Neurite lengths were measured with at least 100 neurons per condition from duplicate wells, and quantified as described previously [18].

After terminal anesthesia by ether hyperaspiration, rats were perfused transcardially with buffered 4% paraformaldehyde. Spinal cords were removed, postfixed overnight, and cryoprotected in buffered 30% sucrose overnight. Tissues were cut into 20-μm sections with a cryostat and mounted on glass slides. Sections were blocked in PBS containing 1% BSA and 10% normal goat serum for immunohistochemical analysis. Sections were then incubated overnight at 4 °C with polyclonal rabbit anti-Iba-1 antibody (Wako Pure Chemical Industries, 1:200) for microglia staining, and monoclonal mouse anti-CD68 antibody (ED1; Chemicon International, 1:100) for activated microglia staining. After rinsing, sections were incubated with the secondary antibody, Alexa Fluor 488, 594-conjugated streptavidin (Invitrogen, 1:400) in PBS with 0.05% Tween20 for 60 min at room temperature.

The midpoint of a lesion was determined by hematoxylin-and-eosin staining of several serial sagittal 20 μm sections. Light intensity and thresholding values were maintained at constant levels for all analyses by a computer-driven microscope stage. All the image analyses shown hereafter were performed using spinal cord samples prepared from five sagittal sections at 20 μm intervals (a midsagittal section and two sections on either side of the midline, which was identified by the appearance of the central tube). In all sagittal sections shown here, the left side is rostral. The measured area was set between 10 mm caudal and 10 mm rostral to the lesion center.

Eight weeks after injury, descending CST fibers were labeled with biotin-dextran amine (BDA; 10% in saline, 3.5 μl per cor-

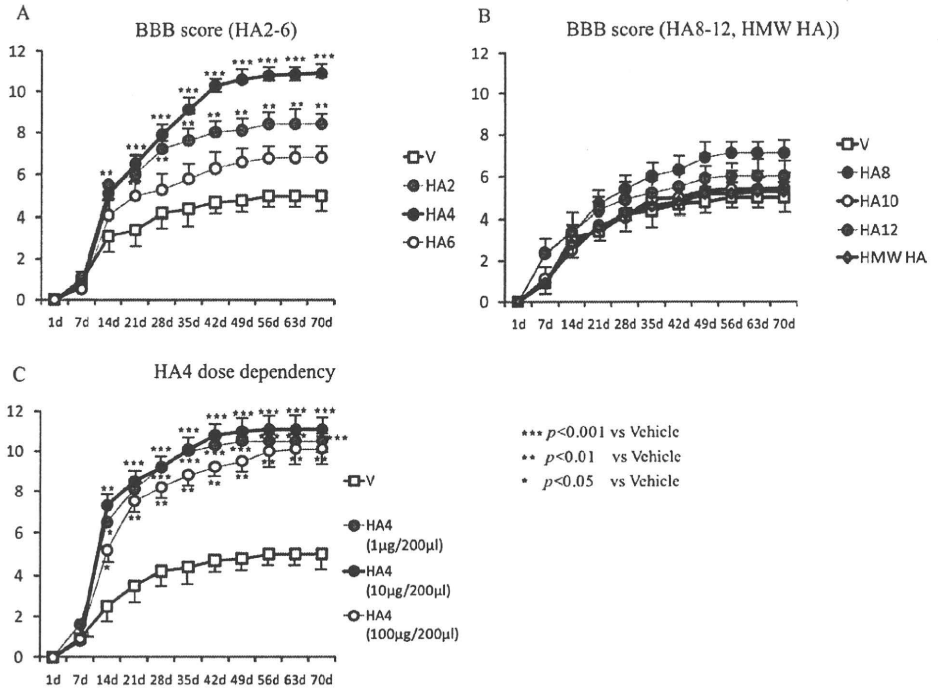

Fig. 1. Motor function recovery promoted by HA4. BBB score data after spinal cord injury. Functional improvements in all groups showed significant difference ($p < 0.001$, F value = 65.05: repeated measure ANOVA). Recovery in HA4 was significant in post hoc Tukey's test ($p = 0.012$). (A) Results of HA2-6 and vehicle. Data represent the means ± SEM. $^{**}p < 0.01$; $^{***}p < 0.001$ vs. vehicle control (t-test) (vehicle, $n = 8$; HA2, $n = 9$; HA4, $n = 7$; HA6, $n = 5$). (B) Results of HA8-12, HMW-HA, and vehicle (HA8, $n = 10$; HA10, $n = 10$; HA12, $n = 8$; HMW-HA, $n = 7$). (C) Motor function recovery after spinal cord injury in rats treated with HA4 at various doses. Data represent the means ± SEM. $^{*}p < 0.05$; $^{**}p < 0.01$; $^{***}p < 0.001$ vs. the vehicle control (vehicle, $n = 8$; HA4 [1 μg/200 μl], $n = 9$; HA4 [10 μg/200 μl], $n = 8$; HA4 [100 μg/200 μl], $n = 8$).

tex; Invitrogen) injected while the animals were anesthetized into the left and the right motor cortices (coordinates: 2 mm posterior to the bregma, 2 mm lateral to the bregma, 1.5 mm depth). For each injection, 0.25 μl of BDA was delivered for 30 s via a 15–20-μm inner-diameter glass capillary attached to a microliter syringe (ITO). Two weeks after BDA injection, animals were sacrificed by perfusion with PBS followed by 4% paraformaldehyde. Spinal cords were dissected, postfixed overnight in identical fixatives across conditions, and cryopreserved in 30% sucrose in PBS. A 20-mm length of spinal cord 10 mm rostral and 10 mm caudal to the lesion site was embedded in Tissue Tek OCT. These blocks were sectioned in the transverse plane (25 μm). Sections were blocked in PBS with 0.3% TritonX for 4 h, and then incubated for 2 h with Alexa Fluor 488–conjugated streptavidin (Invitrogen, 1:400) in PBS with 0.05% Tween20. Then we obtained serial cross-sections of the spinal cord and quantitatively analyzed distribution of the axons. The degree of BDA uptake was assessed by counting the total number of fibers in the cross-section 10 mm rostral to the lesioned site, where the CST was intact. For quantification of the number of labeled corticospinal axons 10 mm caudal to the lesion site, labeled fibers were counted in the gray matter, the dorsal CST area (i.e., normal locations of the dorsal CST), or the white matter (excluding the dorsal CST area), and that number was divided by the number of labeled corticospinal axons 10 mm above the lesion. Labeled fibers were counted using MetaMorph. Light intensity and thresholding values were maintained at constant levels for all analyses.Statistical analysis was performed with SPSS. Experiments involving two groups were compared via unpaired Student's t-test. Experiments involving more than two groups were compared by multiple-way analysis of variance (ANOVA), followed by post hoc analysis (Tukey's test). For the BBB score, we used repeated-measures ANOVA and Tukey's test. Significance was defined as $p < 0.05$.

We employed a contusion-injury model of the spinal cord to investigate the effects of HA oligosaccharides on neurological function after injury. All HA oligosaccharides were locally infused via osmotic pumps for two weeks. Our decision to use 10 μg/200 μl for the HA dose was based on former reports of tumorigenesis [8]. Motor function recovery was evaluated using the BBB score.

As shown Fig. 1A and B, functional improvements in all groups showed a significant difference ($p < 0.001$, F value = 65.05: repeated measure ANOVA). The difference between HA4 and vehicle was significant ($p = 0.012$: Post hoc Tukey's test). However, neither the other HA oligosaccharides (i.e., HA6, 8, 10 and 12) nor the HMW-HA were associated with such an ameliorative effect. The HA4 dose was effective at least within the range of 1 and 100 μg/200 μl (Fig. 1C).

To obtain histological evidence in support of the motor function recovery promoted by HA4, we performed anterograde labeling of the cortico-spinal tract (CST) with BDA dye. We observed that BDA-positive fibers filled the CST 10 mm rostral to the lesion (Fig. 2A), and the number of BDA-positive fibers was comparable between HA4-treated and vehicle-control groups (Fig. 2B). In contrast, there were significantly more BDA-positive fibers in the HA4-treated group in the region 10 mm caudal to the lesion, particularly in the gray matter of this region (Fig. 2C and D). Thus, HA4 treatment contributed to axonal regeneration/sprouting after SCI.

Iba-1-positive cell accumulation in the lesion was significantly reduced in HA4-treated rats 2 weeks after SCI, although there was no difference between HA4 treatment and vehicle control 1 week after injury (Fig. 2E). We further performed staining for ED1 (CD68), as it is known as a marker for proinflammatory activated microglia/macrophage [12,15]. ED1-positive cell accumulation in the lesion was significantly reduced in HA4-treated rats both 1 and 2 weeks after SCI (Fig. 2F). Higher magnification images of double-staining with Iba-1 and ED1 demonstrate that Iba-1-positve cells

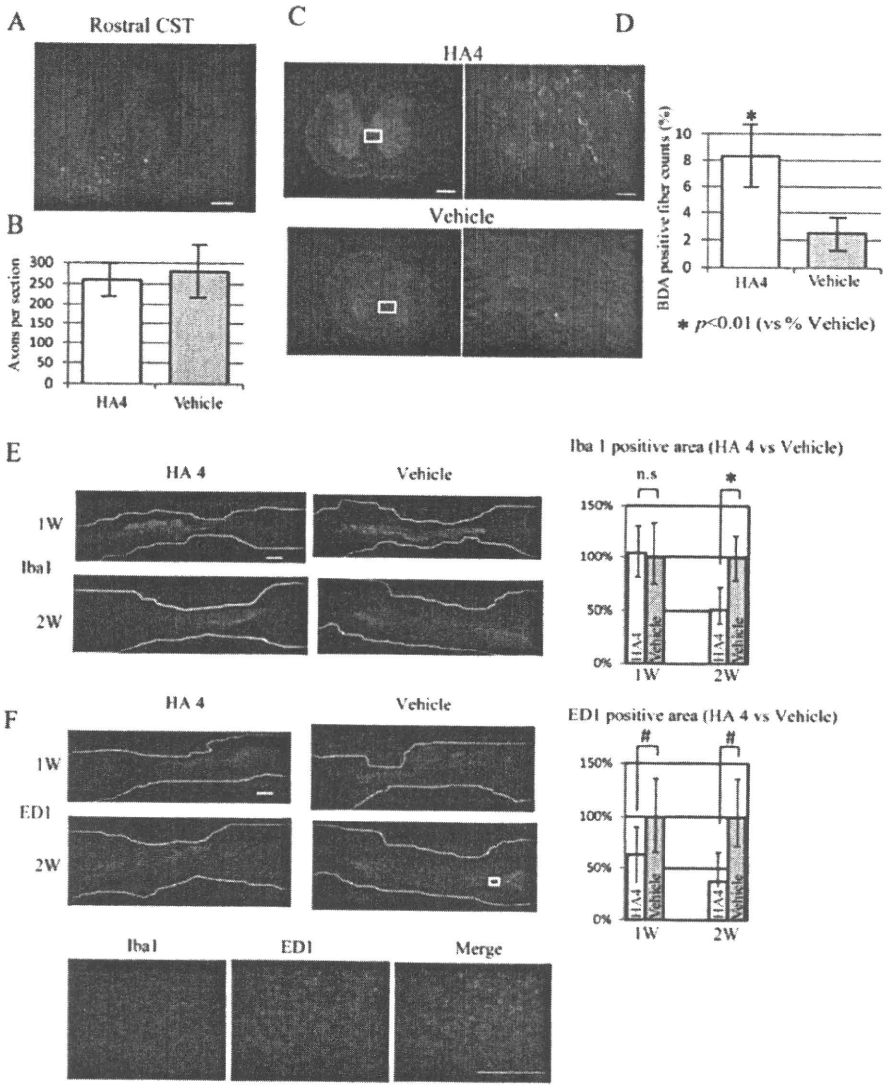

Fig. 2. HA4 treatment enhances axonal regeneration/sprouting and suppresses accumulation of activated microglia. Five rats from each group were examined. (A) Representative transverse sections of labeled corticospinal axons 10-mm rostral from the lesion site 10 weeks after spinal cord injury. Bar, 100 μm. (B) Quantification of labeled corticospinal axons. No significant difference was observed between the HA4 and vehicle-treatment groups. CST, cortico spinal tract. (C) Representative transverse sections of spinal cord obtained from 10-mm caudal from the lesion site 10 weeks after spinal cord injury. Right, magnified images of boxed areas in gray matter. Bar, 500 μm for the left panel; 50 μm for the right panel. (D) The ratio of labeled corticospinal axons 10 mm caudal vs. 10 mm rostral from the lesion site. (E) Expression profile and quantification of Iba-1-reactive microglia 1 and 2 weeks after spinal cord injury in HA4-administered and vehicle-treated rats. Bar, 500 μm. *$p = 0.02$. (F) Expression profile and quantification of ED1-reactive activated microglia 1 and 2 week after SCI in HA4-administered and vehicle-treated rats. Lower panels, magnified images double staining for Iba-1 and ED1 of the boxed area in (F). Bar, 200 μm. #$p < 0.05$. Measured area was set between 10 mm caudal and 10 mm rostral to the lesion center.

were morphologically activated microglia, and that a part of Iba-1-positive cells were positive for ED1 (Fig. 2F). Therefore, HA4 exerted inhibitory effects on activated microglial/macrophage recruitment in these lesions.

Functional recovery after neuronal injury can be partly explained by axonal regeneration/sprouting. Therefore, we examined whether or not HA oligosaccharides exert direct effects on neurite outgrowth. However, no HA oligosaccharides examined were associated with elongation of neurites (Fig. 3A).

It is known that adult CNS neuronal axons regenerate very little after injury, mostly due to upregulation of inhibitory molecules. Chondroitin sulfate proteoglycans are among the strongest inhibitory cues, and have been extensively studied to uncover the underlying mechanisms of inhibition that might suggest directions for the development of novel therapies. Therefore, we next examined whether or not HA oligosaccharides can reverse the proteoglycan-mediated inhibition of neurite outgrowth. However, the oligosaccharides investigated here did not show the capacity to reverse neurite-outgrowth inhibition induced by proteoglycans (data not shown).

We next examined neuroprotective effects of HA oligosaccharides against NMDA excitotoxicity. Each HA oligosaccharide was added to primary-cultured CGNs at 14 days, and NMDA was administered 24 h post-HA oligosaccharide treatment. After another 24 h culture period, cell viability in the cultures was assessed. When cultured CGNs were immunostained with PI and calcein-AM, only HA4 (i.e., not the other oligosaccharides examined) was associated with loss of fewer PI-positive cells ($p = 0.02$) (Fig. 3B). As PI staining is indicative of necrotic cell death, we next examined another cell-death marker, LDH release. LDH activity of

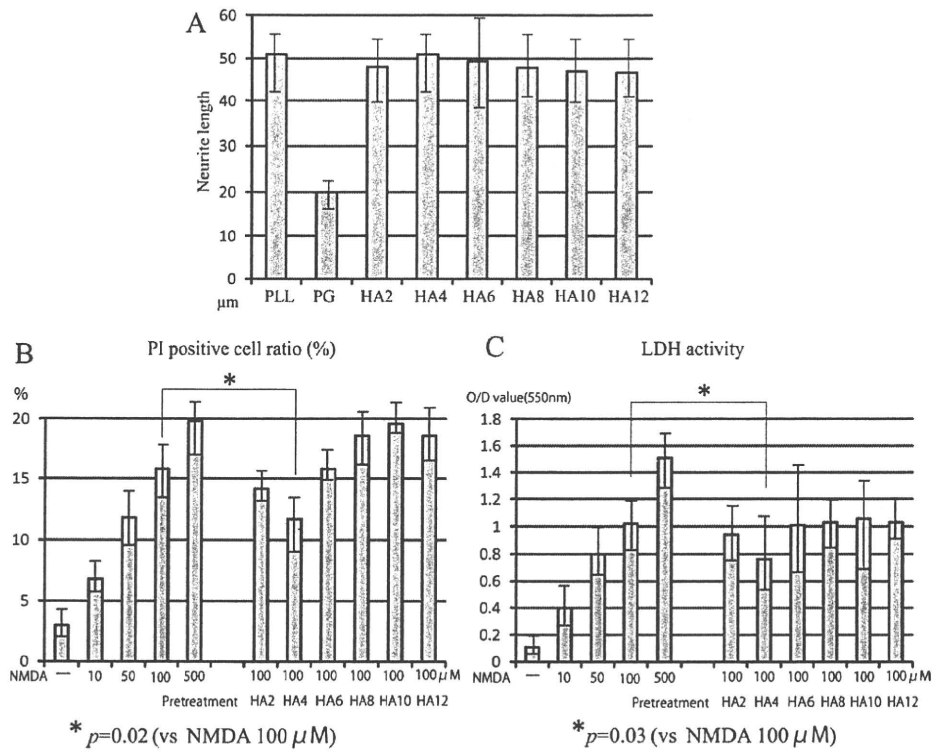

Fig. 3. Effects of HA oligosaccharides on neurite outgrowth and neuroprotection. (A) P8 rat cerebellar granule neurons were cultured on poly-L-lysine (PLL), proteoglycan extracted from chicken brain tissues (PG) or HA. Data represent average neurite length ± SD. (B) Data represent the average ratio of PI-positive cells. *$p = 0.02$ vs. 100 μM NMDA administration. (C) Lactate dehydrogenase (LDH) activity in culture media 24 h after NMDA administration. Data represent the average optimal density value (550 nm). *$p = 0.03$ vs. 100 μM NMDA administration. Results of (B) and (C) are represented as means ± SD ($n = 3$, where n indicates the number of wells per plate for each of three experimental conditions).

HA4-treated neurons was significantly lower than that of 100 μM NMDA-treated neurons ($p = 0.03$) (Fig. 3C). These results indicate that HA4 exerts a neuroprotective effect against NMDA-induced excitotoxicity.

In this study, we demonstrated for the first time that an HA oligosaccharide, HA4, improved motor function recovery after SCI. As HA4 exerted protective effects against NMDA-induced excitoneurotoxicity in primary CGNs, but did not generate any neurite outgrowth-promoting activity, the *in vivo* therapeutic effects of HA4 may be in part due to its neuroprotective activities. Although we could not find a cause-consequence relationship between HA4 administration and the reduced recruitment of microglia/macrophage into the lesions, reduced recruitment of Iba-1-positive cells and ED1-positive cells into lesions might also contribute to the functional recovery promoted by HA4.

Hascall and Heinegrad demonstrated that the smallest HA that binds to proteoglycans is HA10 [6]. Thus, oligosaccharides longer than HA10 might play a competitive role in the interaction between HA and proteoglycans, whereas HA4 may not. Furthermore, HA6 is the minimum oligomer size for efficiently occupying the HA binding site of CD44, a well-known receptor for HA [10]. HA4 might be recognized by an unknown receptor on cells in the CNS, and by this mechanism exert its neuroprotective effects. It is noteworthy that cells other than CNS cells can be targets for HA4. As opposed to other oligomers, only HA4 upregulates Hsp72 expression by enhancing HSF1 activation under conditions of hyperthermia; and consequently HA4 plays a crucial role in suppressing cell death [22]. Moreover, HA2-4 can also induce I-B expression in macrophages [13].

It has not yet been extensively investigated whether or not hyaluronidase is effective on neuronal network rearrangement *in vivo*; the reported results have remained controversial. Struve et al. reported HA degradation soon after SCI, and found that injection of hyaluronidase into the normal spinal cord leads to proliferation of astrocytes [19]. Therefore, HA degradation might trigger gliosis after neuronal injury. In contrast, Moon et al. reported that partial degradation of HA with this enzyme can enhance local sprouting of cut CNS neurons (in the nigrostriatal tract), but long-distance regeneration fails where residual HA-binding CSPGs remain [11]. Furthermore, it has been recently reported that hyaluronidase can promote short-term synaptic plasticity by enhancing lateral mobility of AMPA-type glutamate receptor on the spine [4]. Although our present data demonstrative of the promotion of motor function recovery by an HA oligosaccharide do not necessarily indicate that degradation products induced by hyaluronidase *in vivo* have neuroprotective activity, HA4 must be included among HA-degradation products. The present results therefore suggest the intriguing possibility that HA4 could be incorporated into a useful strategy for the treatment of neuronal injuries.

Acknowledgements

The authors gratefully acknowledge Prof. Nobuyuki Hamajima, Department of Preventive Medicine, Nagoya University, for supervising all statistical analyses, and Hiroshi Maeda of Seikagaku Corporation for overall assistance in preparation of the HA oligosaccharides.

References

[1] D.M. Basso, M.S. Beattie, J.C. Bresnahan, A sensitive and reliable locomotor rating scale for open field testing in rats, J. Neurotrauma 12 (1995) 1–21.

[2] M.R. Celio, I. Blumcke, Perineuronal nets—a specialized form of extracellular matrix in the adult nervous system, Brain Res. Brain Res. Rev. 19 (1994) 128–145.

[3] M.R. Celio, R. Spreafico, S. De Biasi, L. Vitellaro-Zuccarello, Perineuronal nets: past and present, Trends Neurosci. 21 (1998) 510–515.

[4] R. Frischknecht, M. Heine, D. Perrais, C.I. Seidenbecher, D. Choquet, E.D. Gundelfinger, Brain extracellular matrix affects AMPA receptor lateral mobility and short-term synaptic plasticity, Nat. Neurosci. 12 (2009) 897–904.

[5] N. Gogolla, P. Caroni, A. Luthi, C. Herry, Perineuronal nets protect fear memories from erasure, Science 325 (2009) 1258–1261.

[6] V.C. Hascall, D. Heinegard, Aggregation of cartilage proteoglycans. II. Oligosaccharide competitors of the proteoglycan–hyaluronic acid interaction, J. Biol. Chem. 249 (1974) 4242–4249.

[7] M.E. Hatten, Neuronal regulation of astroglial morphology and proliferation in vitro, J. Cell Biol. 100 (1985) 384–396.

[8] K. Hosono, Y. Nishida, W. Knudson, C.B. Knudson, T. Naruse, Y. Suzuki, N. Ishiguro, Hyaluronan oligosaccharides inhibit tumorigenicity of osteosarcoma cell lines MG-63 and LM-8 in vitro and in vivo via perturbation of hyaluronan-rich pericellular matrix of the cells, Am. J. Pathol. 171 (2007) 274–286.

[9] N. John, H. Krugel, R. Frischknecht, K.H. Smalla, C. Schultz, M.R. Kreutz, E.D. Gundelfinger, C.I. Seidenbecher, Brevican-containing perineuronal nets of extracellular matrix in dissociated hippocampal primary cultures, Mol. Cell. Neurosci. 31 (2006) 774–784.

[10] J. Lesley, V.C. Hascall, M. Tammi, R. Hyman, Hyaluronan binding by cell surface CD44, J. Biol. Chem. 275 (2000) 26967–26975.

[11] L.D. Moon, R.A. Asher, J.W. Fawcett, Limited growth of severed CNS axons after treatment of adult rat brain with hyaluronidase, J. Neurosci. Res. 71 (2003) 23–37.

[12] D.M. Mosser, J.P. Edwards, Exploring the full spectrum of macrophage activation, Nat. Rev. Immunol. 8 (2008) 958–969.

[13] P.W. Noble, C.M. McKee, M. Cowman, H.S. Shin, Hyaluronan fragments activate an NF-kappa B/I-kappa B alpha autoregulatory loop in murine macrophages, J. Exp. Med. 183 (1996) 2373–2378.

[14] T. Pizzorusso, P. Medini, N. Berardi, S. Chierzi, J.W. Fawcett, L. Maffei, Reactivation of ocular dominance plasticity in the adult visual cortex, Science 298 (2002) 1248–1251.

[15] S.D. Ricardo, H. van Goor, A.A. Eddy, Macrophage diversity in renal injury and repair, J. Clin. Invest. 118 (2008) 3522–3530.

[16] A. Schousboe, A. Frandsen, J. Drejer, Evidence for evoked release of adenosine and glutamate from cultured cerebellar granule cells, Neurochem. Res. 14 (1989) 871–875.

[17] L.S. Sherman, S.A. Back, A 'GAG' reflex prevents repair of the damaged CNS, Trends Neurosci. 31 (2008) 44–52.

[18] R. Sivasankaran, J. Pei, K.C. Wang, Y.P. Zhang, C.B. Shields, X.M. Xu, Z. He, PKC mediates inhibitory effects of myelin and chondroitin sulfate proteoglycans on axonal regeneration, Nat. Neurosci. 7 (2004) 261–268.

[19] J. Struve, P.C. Maher, Y.Q. Li, S. Kinney, M.G. Fehlings, C.t. Kuntz, L.S. Sherman, Disruption of the hyaluronan-based extracellular matrix in spinal cord promotes astrocyte proliferation, Glia 52 (2005) 16–24.

[20] H. Takahashi-Iwanaga, T. Murakami, K. Abe, Three-dimensional microanatomy of perineuronal proteoglycan nets enveloping motor neurons in the rat spinal cord, J. Neurocytol. 27 (1998) 817–827.

[21] A. Tawada, T. Masa, Y. Oonuki, A. Watanabe, Y. Matsuzaki, A. Asari, Large-scale preparation, purification, and characterization of hyaluronan oligosaccharides from 4-mers to 52-mers, Glycobiology 12 (2002) 421–426.

[22] H. Xu, T. Ito, A. Tawada, H. Maeda, H. Yamanokuchi, K. Isahara, K. Yoshida, Y. Uchiyama, A. Asari, Effect of hyaluronan oligosaccharides on the expression of heat shock protein 72, J. Biol. Chem. 277 (2002) 17308–17314.

Biochemical and Biophysical Research Communications 401 (2010) 463–468

Contents lists available at ScienceDirect

Biochemical and Biophysical Research Communications

journal homepage: www.elsevier.com/locate/ybbrc

Keratan sulfate suppresses cartilage damage and ameliorates inflammation in an experimental mice arthritis model

Masatoshi Hayashi [a,b,*], Kenji Kadomatsu [a], Naoki Ishiguro [b]

[a] Department of Biochemistry, Nagoya University Graduate School of Medicine, 65 Tsuruma-cho, Showa-ku, Nagoya 466-8550, Japan
[b] Department of Orthopedics, Nagoya University Graduate School of Medicine, 65 Tsuruma-cho, Showa-ku, Nagoya 466-8550, Japan

ARTICLE INFO

Article history:
Received 4 September 2010
Available online 25 September 2010

Keywords:
Keratan sulfate
Arthritis
Cartilage degradation
Rheumatoid arthritis

ABSTRACT

Proteoglycans bearing keratan sulfate (KS), such as aggrecan, are components of the human cartilage extracellular matrix (ECM). However, the role of KS in influencing cartilage degradation associated with arthritis remains to be completely understood. KS side chains of the length found in human cartilage are not found in murine skeletal tissues. Using a murine model of inflammatory polyarthritis and cartilage explants exposed to interleukin-1α (IL-1α), we examined whether administering KS could influence intraarticular inflammation and cartilage degradation. Acute arthritis was induced by intravenous administration of an anti-type II collagen antibody cocktail, followed by an intraperitoneal injection of lipopolysaccharide. This treatment was followed by an intraperitoneal KS administration in half of the total mice to evaluate the therapeutic potential of KS for ameliorating arthritis. To investigate the therapeutic potential *ex vivo*, we examined cartilage fragility by measuring IL-1α-induced aggrecan release from cartilage explants treated with or without KS. Intraperitoneal KS administration ameliorated arthritis in DBA/1J mice. The aggrecan release induced by IL-1α was less in cartilage explants containing media with KS than in those without KS. Our data indicate that exogenous KS ameliorated arthritis *in vivo* and suppressed cartilage degradation *ex vivo*. KS may have important therapeutic potential in the treatment of inflammatory arthritis. The mechanism responsible for this requires further investigation, but KS may become a novel therapeutic agent for treating inflammatory diseases such as rheumatoid arthritis.

1. Introduction

Rheumatoid arthritis (RA) is a major musculoskeletal disorder involving joint destruction of articular cartilage and subchondral bone resulting in a negative impact on the quality of life [1]. Articular cartilage is composed of chondrocytes embedded in an extracellular matrix (ECM), which provides the biomechanical factors essential for articular movement, especially those for resisting compressive forces. The two major components of cartilage ECM are type II collagen and proteoglycans. A predominant component of the latter is aggrecan, which is further composed of two types of glycosaminoglycan (GAG) side chains in humans, namely chondroitin sulfate (CS) and keratan sulfate (KS). GAGs contain sulfate residues and are thus negatively charged. This negative charge facilitates water retention in ECM, enabling the cartilage to resist compressive forces.

CS combined with glucosamine salts provides symptomatic relief and chondroprotection [2–4]. However, whether KS has similar properties during articular cartilage degradation remains unclear. The role of KS side chains in articular cartilage degradation remains to be understood with regard to arthritis [5].

In general, KS side chains of the type found in human cartilage and other mammals are not found in the skeletal tissues of mice and rats [6]. However, human articular cartilage has smaller amounts of KS than CS, and higher rates of KS/CS changes occur in older individuals [7,8]. Thus, we hypothesized that KS affect changes in articular cartilage characteristics of arthritis and may be chondroprotective in humans based on their longevity compared to rats and mice.

Murine anti-type II collagen antibody-induced arthritis and cartilage organ culture are widely used to study the mechanisms of cartilage degradation associated with inflammatory joint diseases such as RA [9,10]. In this study, we employed these arthritis models to verify the role of KS in cartilage degradation in arthritis.

Molecular fragments of cartilage are antigenic and can stimulate an arthritic response [11–14]. Thus, lesser the cartilage breaks down and releases fragments into synovial fluid, lesser is the severity of arthritis in the joint. Based on this, if KS has

Abbreviations: KS, keratan sulfate; CS, chondroitin sulfate; GAG, glycosaminoglycan.

* Corresponding author at: Department of Orthopedics, Nagoya University Graduate School of Medicine, 65 Tsuruma-cho, Showa-ku, Nagoya 466-8550, Japan.
E-mail address: hayashimasatoshi@hotmail.com (M. Hayashi).

0006-291X/$ - see front matter © 2010 Elsevier Inc. All rights reserved.
doi:10.1016/j.bbrc.2010.09.082